ALLOPURINOL BLOCKS THE FORMATION AND PROGRESSION OF AORTIC ANEURYSM IN A MOUSE MODEL OF MARFAN SYNDROME

Isaac Rodríguez-Rovira[1,*], Karo De Rycke[1,*,¶], Cristina Arce[1,*,†], Belén Pérez[2], Aitor Carretero[3], Marc Arbonés[1], Gisela Teixidò-Turà[4], Mari Carmen Gómez-Cabrera[3], Victoria Campuzano[1,5], Francesc Jiménez-Altayó[2] and Gustavo Egea[1,#]

[1] Department of Biomedical Sciences, University of Barcelona School of Medicine and Health Sciences and IDIBAPS, 08036 Barcelona, Spain.

[2] Department of Pharmacology, Toxicology and Therapeutics, Neuroscience Institute, School of Medicine, Autonomous University of Barcelona, 08193 Cerdanyola del Vallès, Spain.

[3] Department of Physiology, Faculty of Medicine, University of Valencia, CIBERFES, Fundación Investigación Hospital Clínico Universitario/INCLIVA, Valencia, Spain.

[4] Department of Cardiology, Hospital Universitari Vall d'Hebron, Barcelona, Spain. CIBER-CV, Vall d'Hebron Institut de Recerca (VHIR), Barcelona, Spain

[5] Centro de Investigación Biomédica en Red de Enfermedades Raras (CIBERER), ISCIII, Spain.

[#] Corresponding author: Gustavo Egea, Dept. Biomedicina, Facultat de Medicina, Universitat de Barcelona, c/ Casanova 143, 08036 Barcelona, Spain, +34648557759, gegea@ub.edu

* These authors contributed equally to this work.

¶ Present address: Center for Medical Genetics, Department of Biomolecular Medicine, Ghent University, Ghent, 9000, Belgium.

† Present address: Dept of Biology, University of Padova, via Ugo Bassi 58b, Padova, Italy.

The authors have declared that no conflict of interest exists.

ABSTRACT (200 words)

We reported elevated reactive oxygen species (ROS) formation and NADPH oxidase NOX4 upregulation in MFS mice and patient aortic samples. Here we address the contribution of xanthine dehydrogenase (XDH) which catabolizes purines into uric acid plus ROS. In MFS patients, protein levels of the oxidase form (XO) of XDH increased in the dissected aneurysm. XDH mRNA and protein expression levels increased in the aorta of young but not older MFS mice. The protein and enzymatic activity of XO increased with respect to the dehydrogenase. The XDH inhibitor allopurinol blocked the progression of the aortic root aneurysm in MFS mice, and it was also protective when administrated before the appearance of aneurysm. Elastic fiber fragmentation, fibrotic remodeling, nuclear translocation of pNRF2, increased 3'-nitrotyrosine levels in the aortic tunica media, and endothelial dysfunction were all prevented by allopurinol. MFS ascending aorta showed a large overproduction of H_2O_2 which did not occur in allopurinol-treated MFS mice. Allopurinol mediated the inhibition of the MFS aortopathy inhibiting ROS overproduction without altering uric acid plasma levels. This study strengthens that redox stress is an important determinant of aortic aneurysm development in MFS and supports a clinical trial for allopurinol in the pharmacological treatment of MFS aortopathy.

Nonstandard abbreviations

ALO: allopurinol; CRCs: cumulative concentration-response curves; 3-NT: 3'nitrotyrosine; PA: palliative experimental treatment with allopurinol; PE: preventive experimental treatment with allopurinol; PE-ALO: PE treatment and thereafter allopurinol withdrawal.

INTRODUCTION

Marfan syndrome (MFS) is a relatively common inherited rare disease of the connective tissue (1:5,000), caused by mutations in the gene encoding the extracellular matrix glycoprotein fibrillin-1 *(1)*. This multisystem disease mainly affects the skeleton (abnormally long bones and spine deformations), eyes (lens dislocation) and aortic root aneurysm. The latter commonly leads to aortic dissection and rupture, the main reason for reduced life expectancy in patients *(2)*.

Reactive oxygen species (ROS) are essential mediators of cell physiology, modulating the activity of many signaling molecules (redox signaling). ROS are highly reactive chemicals formed from oxygen (O_2), including hydrogen peroxide (H_2O_2), superoxide (O_2^-), and hydroxyl radical (OH^-) as the primary, most frequently formed. However, when ROS are chronically overproduced, they contribute to pathogenesis (redox stress), causing transient or permanent damage to nucleic acids, proteins, and lipids *(3)*. In the cardiovascular system, ROS are involved, among other dysfunctions, in the development of aortic abdominal aneurysms (AAA) through the regulation of inflammation induction, matrix metalloproteinase (MMPs) expression, vascular smooth muscle cell (VSMC) apoptosis and phenotypic changes and modifying extracellular matrix properties *(4–10)*, but much less understood in thoracic aortic aneurysm (TAA) of genetic origin, such as in MFS and Loeys-Dietz syndrome (LDS) *(11)*. We and others have shown that ROS production is increased in MFS *(12–18)* , although

their sources and impact on the formation and/or progression in either human or murine MFS aortic aneurysms is still not well established *(19, 20)*. We reported the involvement of upregulated NADPH (nicotinamide adenine dinucleotide phosphate) oxidase 4 (NOX4) both in human and mouse MFS aortic samples and cultured VSMC *(17)*. Nonetheless, besides NOX4, another important source of ROS in the cardiovascular system is xanthine dehydrogenase (XDH), which also goes by the alias xanthine oxidoreductase (XOR) *(21)*.

XDH/XOR is a rate limiting enzyme involved in the final steps of purine degradation, particularly in the conversion of hypoxanthine into xanthine and xanthine into urate. XDH/XOR is present in two interchangeable protein forms: dehydrogenase (XDH) and oxidase (XO), having the former greater abundance and affinity for NAD^+. XDH is converted into XO by oxidation of the sulfhydryl residues or by proteolysis *(22)*. The XO-mediated enzymatic reaction is associated with the production of large amounts of O_2^- as well as H_2O_2 *(23, 24)*. XDH conversion into XO is favored by hypoxia, low pH, ischemia, or the presence of H_2O_2 itself *(24)*. XDH is present in the bloodstream and in the liver, intestine, myocardium, and vascular endothelium bound to cell surface glycosaminoglycans, and the enhancement of endothelium attached XDH favors the local production of ROS with subsequent endothelial dysfunction *(25)*. Increased levels of XDH have been reported in aortic samples from adult MFS mice *(26)* and LDS patients *(27)*, yet the participation of XDH in TAA pathogenesis remains poorly understood.

Concomitantly to ROS production, XDH generates uric acid (UA), which in humans and great apes can pathologically accumulate in the plasma and some tissues. In rodents, UA is rapidly catabolized by uricase to allantoin, which is much more water soluble than UA *(28)*. In humans, given the evolutionary loss of the uricase gene (*Uox*), UA can chemically react with O_2^- to generate allantoin. Allantoin is increased in the serum of chronic heart failure patients and has been proposed as a biomarker for oxidative stress and a possible *in vivo* indicator of free radical concentrations in humans *(29, 30)*.

Several epidemiological studies suggest a relationship between elevated serum UA and cardiovascular risk, but this association remains controversial *(31, 32)*. UA has a dual role in redox biology, acting as an antioxidant (both *in vitro* and *in vivo*) accounting for as much as 50% of the total antioxidant capacity of biological fluids in humans *(33, 34)*. However, when UA accumulates in the cytoplasm or in acidic/hydrophobic milieu, it acts as a pro-oxidant promoting redox stress *(35, 36)*. UA was found in the wall of human aortic aneurysms and atherosclerotic arteries *(37)* and there is a positive correlation between serum UA levels and aortic dilation and dissection *(38, 39)*. Epidemiologic and biochemical studies on UA formation have demonstrated that it is not only UA itself that leads to worse prognosis and increased cardiovascular events, but also ROS formed during XDH activity. These XDH-derived O_2^- easily interact with endothelial cell-generated nitric oxide (NO) forming peroxynitrite, which in turn diffuses to the adjacent aortic media layer. Here, the more ROS formed, the more irreversible chemical modifications to nucleic acids, proteins (tyrosine nitration), and lipids (lipid peroxidation) are

produced *(3, 40, 41)*. Therefore, the resulting combined action of excessively formed UA and free radicals, along with enhanced XDH activity, could contribute to oxidative stress-linked cardiopathological events *(31, 32, 42)*.

We hypothesized that UA and/or ROS derived from an abnormal activity of aortic XDH participates in the formation and/or progression of the aortic aneurysm in MFS jointly with upregulated NOX4 *(17, 43)*, where TGFβ turns out to be directly or indirectly pivotal. Thus, the dual aim of this study was firstly to investigate in detail the participation of XDH as a source of ROS and oxidative stress in MFS, and secondly, to evaluate the effectiveness of the XDH inhibitor allopurinol (ALO) *(44)* on the formation and progression of MFS-associated aortopathy. We report that XDH expression and activity are augmented in MFS aorta of patients and young mice. ALO fully prevented both the formation and progression of the aortic aneurysm as well as the associated aortic wall degeneration. These effects were not mediated by changes in UA levels, which strikingly remained unaltered with age, but rather because ALO is primarily acting as a scavenger of ROS. Our results definitively highlight that redox stress is a significant driving force of MFS aortopathy and propose the popular and widely prescribed drug ALO as a feasible pharmacological therapeutic agent to prevent or attenuate aortic aneurysm progression in MFS.

RESULTS

The XO protein form is enhanced in the aorta of MFS patients.

To investigate the contribution of XDH in MFS, we first explored whether XDH expression is altered in the aorta of MFS patients subjected to aortic reparatory

surgery. We evaluated by western blotting XDH and XO protein forms both in the aneurysmal (dilated) and the adjacent and non-aneurysmal (non-dilated), aortic regions compared with virtually healthy aortae from heart donors. XDH protein is revealed as a strongly labeled single band of ~150 kDa that corresponds to the XDH protein form itself, and a lower molecular weight band of ~50 KDa corresponding to the XO form (Fig. 1). The latter is generated from *in vivo* XDH proteolysis, reflecting the characteristic unbalanced conversion between both enzymatic forms. Compared with the healthy aorta, the aneurysmal aortic area of Marfan individuals (both non-dilated and dilated zones) showed an increase of the XO protein form in detriment of the XDH reaching statistical significance in the non-dilated area of the aneurysm compared to the dilated zone ($P \leq 0.0051$ and $P \leq 0.052$, respectively; panel below of Fig. 1).

XDH expression and XO enzymatic activity are both increased in the aorta of MFS mice.

We next evaluated whether *XDH* mRNA and protein levels as well as enzymatic activity were also altered in the MFS mouse (*Fbn1*$^{C1041G/+}$) aorta. We evaluated *XDH* mRNA expression by RT-PCR (Table S1) in 3- and 6-month-old WT and MFS mice, ages in which the aortic root growth ratio is larger *(45)*. Aortae from 3-month-old MFS mice showed a significantly increased *XDH* transcripts compared with age-matched WT animals. This increase was not observed in older mice (6-month-old) (Fig. 2A).

As observed in human aortae, mouse XDH aortic protein is also revealed as a strongly labeled single band of ~150 kDa and a lower molecular weight band of ~50 KDa corresponding to the XO form (left panel in Fig. 2B). As positive control, we

used mouse liver (left panel in Fig. 2B, liver lane) *(46)*. In agreement with transcripts levels, only aortic lysates from 3-month-old MFS mice showed an increased XO/XDH protein ratio compared with WT lysates (right panel in Fig. 2B). Immunohistochemistry with anti-XDH antibodies confirmed the significant increased expression of XDH in both the intima and media layers of MFS mice compared with their WT littermates (Fig. 2C).

To further support the greater presence of XDH in MFS aorta and to differentiate the functional contribution of the XDH and XO protein forms, we measured their respective enzymatic activities *(47)* in liver as positive control (Fig. S1) and aorta lysates (left panel in Fig. 2D). In MFS aorta, the XO/XDH enzymatic activity ratio was significantly higher in 3-month-old but not in 6-month-old mice (right panel in Fig. 2D). Therefore, results indicate the major participation of the XO form and provide new information to that previously reported that XDH was upregulated in MFS mouse aorta *(14)*.

Allopurinol prevents the formation and progression of aortic aneurysm in MFS mice.

The observation that XDH is upregulated in young mouse and human MFS aortae, suggests its contribution to oxidative stress in MFS. Therefore, we hypothesized that the inhibition of its activity, with the consequent reduction of UA and ROS production should ameliorate aortic aneurysm progression. To test this hypothesis, we treated WT and MFS mice with the XDH inhibitor allopurinol (ALO). ALO is a safe, well-tolerated, and cheap routinely prescribed drug to treat hyperuricemia in hyperuricemic and hypertensive patients *(44, 48)*. Thus, we first palliatively treated

2-month-old mice with ALO for a period of 16 weeks until 6 months of age (PA1; Fig. S2) and then evaluated aneurysm progression by ultrasonography. ALO significantly reduced the enlarged aortic root diameter occurring in MFS mice, the diameter obtained being highly similar to WT animals (Fig. 3A and Table S2). Note that ALO did not cause any alteration in the aortic root diameter of WT mice. Moreover, no sex differences were observed regarding the effectiveness of allopurinol (Table S2)

We also evaluated the aortic wall organization in these mice by histomorphology, quantifying the number of large elastic fiber ruptures as previously defined *(45)*. ALO treatment in MFS mice caused an apparent normalization of elastic fiber organization and integrity, their overall morphology being indistinguishable from non-treated WT animals (Fig. 3B).

ALO has also been safely administered during the late stages of pregnancy, demonstrating efficiency in reducing uric acid, hypertension, and oxidative stress levels *(49–52)*. Therefore, we next evaluated whether ALO also prevented the formation of the aneurysm. To this aim, ALO was administrated to pregnant and lactating female mice and then to weaning offspring until the age of 3 months (PE; Fig. S2). ALO fully prevented the formation of the aneurysm (Fig 3C and Table S3), also showing a trend to reduce elastic fiber breaks (Fig. 3D).

The inhibition of the aortopathy by allopurinol is reversible after the drug withdrawal.

We next examined whether the progression of the aortopathy inhibited by ALO was permanent or transient. To this end, the 3-month-old animals subjected to the PE treatment with ALO were withdrawn from the drug from 3-months until 6-months-age

(PE-ALO; Fig. S2). There was no statistical difference between the aortic root diameters measured in the latter group of MFS animals and those MFS non-treated with ALO (6 months-age endpoint) (Fig. S3 and Table S4). Despite the absence of statistical significance, note that the median at 6 months-age of treated PE-ALO MFS mice is less than of non-treated PE-ALO MFS animals (1.77±0.02 *vs* 1.84±0.01; Fig. S3 and Table S4), which suggest that the aortic root diameter in the former mice group has still the capacity of expand throughout latter ages. In any case, the result indicates that the inhibitory effect of ALO on the aneurysm is effective while the drug is present.

Allopurinol reduces H_2O_2 levels in MFS ascending aorta altering neither XDH protein levels nor uric acid plasma concentrations.

Next, we investigated the primary mechanism by which ALO so effectively prevents the formation and progression of the aneurysm. Considering that ALO is clinically prescribed to treat hyperuricemia, we first studied whether UA and its catabolite allantoin were altered in the blood plasma of MFS mice following ALO treatments. Strikingly, UA and allantoin plasma levels did not vary with age and neither did their ratio in MFS mice (Fig. S4A-C). As we observed that ALO treatment inhibited the aneurysm formation at 6-months-old MFS mice (PA1), we measured basal UA plasma levels at this age and strikingly remained unaltered (Fig. 4). The possibility that the inhibition of aneurysm progression was mediated by reducing the blood pressure was also discarded since systolic blood pressure values remained unaltered in both treated and non-treated MFS mice (Fig. S5). ALO did not affect XDH expression in the MFS aortic intima and media layers (Fig. S6). This result was

not unexpected as ALO is a hypoxanthine analogue that does not affect XDH expression (*44,48).*

The observation that ALO induces neither the expected fall of UA plasma levels nor a decrease in XDH expression, leaves open the possibility that it acts by reducing the intrinsic high levels of redox stress, as inhibition of XO activity should also reduce ROS production. This is the result of the oxidation process mediated by XO using O_2 as a cofactor generating O_2^-, and the subsequent reoxidation of the fully reduced XO produces H_2O_2 and two O_2^- species for every reduced XO *(53–55)*. The H_2O_2/O_2^- ratio depends on the local O_2 concentration and pH conditions, H_2O_2 being the major ROS produced under aerobic conditions *(55)*, which is precisely what occurs in the heart and the ascending aorta. Therefore, we measured the production of H_2O_2 both in plasma and in ascending aortic tissue. No differences were observed in H_2O_2 plasma levels between WT and MFS mice of different ages (Fig. S7). Nonetheless, since plasma H_2O_2 can come from diverse tissue sources, we next measured *in situ* H_2O_2 formation in freshly isolated ascending aortic rings. Marfan aortic rings from proximal ascending aorta showed much higher levels of H_2O_2 compared to WT (Fig. 5). Of note, this ROS overproduction did not occur in ALO-treated Marfan aortae following the PE treatment (Fig. 5). The increased H_2O_2 levels occurring in Marfan aortic rings was also inhibited when ALO was added *in vitro*. (Fig. S8). Therefore, ALO blocked the MFS-associated overproduction of H_2O_2 in the ascending aorta whether administered *in vivo* or *in vitro*.

Allopurinol prevents oxidative stress-associated injuries in the aortic media of MFS mice.

Reactive nitrogen species (RNS) can be produced due to the interaction of endothelial-generated NO and XDH-induced ROS *(40, 41)*. Peroxynitrite and 3'-nitrotyrosine (3-NT) products are reliable redox stress biomarkers. Immunohistochemical evaluation of 3-NT showed greater levels in the tunica media of MFS aorta. In both PA1 and PE approaches, ALO significantly prevented this increase (Fig. 6A and 6B, respectively).

The nuclear factor erythroid 2-related factor 2 (NRF2) is a key transcription factor that regulates the expression of several antioxidant defense mechanisms. Oxidative stress triggers its phosphorylation (pNRF2), being subsequently translocated to the nucleus to activate the expression response of physiological antioxidant enzymes *(56)*. Thus, we evaluated the nuclear presence of pNRF2 in aortic paraffin sections from WT and MFS mice treated with ALO after PA1 and PE treatments (Fig. 6C and 6D, respectively). Aortic media showed a higher presence of nuclear pNRF2 in MFS than WT VSMC. This result is demonstrative that the MFS aorta suffers redox stress, which in turn triggers the intrinsic endogenous antioxidant response. However, when ALO was administrated to MFS mice, the number of pNRF2 stained nuclei was indistinguishable from WT aorta, regardless the experimental treatment followed. This result is a logical consequence of the ALO-induced inhibition of the oxidative stress occurring in the MFS aorta.

Elastic fiber disruption in the MFS aorta is often accompanied by a compensatory fibrotic remodeling supported by collagen overexpression and/or organization rearrangements occurring mainly in the tunica media *(57–59)*. This remodeling can be visualized under a polarized light microscope in paraffin-embedded aortae cross-sections stained with Picrosirius red. Green and red collagen fibers were observed,

which is illustrative of their different fiber thickness and assembly compaction, and, therefore, of their degree of maturity *(60)*. We observed an increase in collagen fibers in the aortic media of 6-month-old MFS (PA1 treatment), mainly due to a significant increase in immature (green) fibers, which is demonstrative of a fibrotic-like response. This reorganization is not produced after ALO treatment (Fig. 7). In MFS aortae of 3-month-old animals (PE), the changes began to be appreciated, although no significant differences were reached (Fig. S9). Both in PA1 and PE treatments, ALO did not reduce the increased trend of mature (red) collagen fiber formation (Fig. 7 and Fig. S9, respectively).

Allopurinol prevents endothelial dysfunction in MFS ascending aorta.

XO is the ROS source that could mediate alterations in the endothelial-associated vascular function by reducing NO bioavailability via direct interaction with O_2^- *(29,61)*. Previous evidence indicates that the MFS aorta shows endothelial dysfunction *(14, 62, 63)*. Thus, we analyzed the potential therapeutic effects of ALO treatment (PA2; Fig. S2) on endothelial function (Fig. 8). To this aim, we used wire-myography to measure the reactivity of endothelium-intact ascending aortas from 9-month-old MFS mice (Fig. 8A), age at which endothelial dysfunctions were more clearly observed *(63)*. Aortic root diameter was also evaluated by ultrasonography in this mouse subset. As in 3- and 6-month-old MFS mice (Fig. 3), the aneurysm was also inhibited after 28 weeks of ALO treatment (PA2) (Fig. S10 and Table S5). Thereafter, ascending aortae were isolated, and vessels were contracted with KCl to check their functionality. All aortae responded similarly to KCl (Fig. 8B and Table S7). The relaxant response to ACh, mostly mediated by activation of endothelial NOS (NOS3),

is an indicator of endothelial function. Untreated MFS mice showed a reduced sensitivity (pEC_{50}) to endothelium-dependent ACh-induced relaxation compared with WT (the curve shifted to the right in Fig. 8C/asterisks; Table S6), which indicates that ACh-mediated aortic relaxation is impaired in MFS mice. ALO-treated MFS mice showed an ACh-induced relaxation that was indistinguishable from WT animals (pEC_{50} 7.49 ± 0.19 and 7.52 ± 0.10, respectively) (Fig. 8C; Table S6), which proves that ALO treatment normalizes physiological endothelial function levels in MFS mice. To check the participation of the NO/GC/cGMP pathway in the VSMC of untreated MFS mice, we next added increased concentrations of the NO donor sodium nitroprusside (NTP) to pre-contracted aortae with Phe and the non-selective NOS inhibitor L-NAME (Fig. 8A), resulting in similar concentration-dependent vasodilatations in untreated MFS *versus* WT mice (Fig. 8D). These results indicate that the impaired ACh responses in MFS aortae are demonstrative of endothelial dysfunction. No changes in the vasorelaxant response to NTP were observed in ALO-treated MFS mice (Fig. 8D; Table S6). Next, we also evaluated the α_1-associated contractile response of ascending aortae when stimulated with Phe. No changes were observed either between untreated MFS and WT ascending aortae or following ALO treatment (Fig. 8E; Table S7).

DISCUSSION

Despite the significant insights reported over the last two decades regarding the molecular mechanisms that participate in the formation and progression of aortic aneurysm in MFS, current pharmacological approaches (losartan, atenolol, or both together) have been proven to be not sufficient to stop or mitigate aortic aneurysm

progression *(64)*. Keeping this in mind, the aim of our study was, on the one hand, to obtain further insights into the contribution of redox stress in the molecular pathogenesis of aortic aneurysm paying attention to XDH, which like NADPH oxidases, is another important source of ROS. On the other hand, to provide experimental evidence to support a new pharmacological approach targeting XDH-associated oxidative stress in a well-established murine model of MFS (C1041G), which at the same time could also be assayed in a relatively straightforward manner in patients in a later stage.

The main findings of this article are the following: (i) XDH is overexpressed in the ascending aorta of MFS patients and of young (3 month-old) MFS mice; (ii) this upregulation is accompanied by increased enzymatic activity of the oxidase (XO) over the dehydrogenase (XDH) form; (iii) XDH upregulation and overactivation in the aorta increases ROS production (H_2O_2) in aortic rings without changes in plasma UA levels; (iv) the specific XDH inhibitor ALO prevents the formation and progression of aortic root dilation in MFS mice without changes in UA levels or changes in blood pressure; (v) this inhibitory effect is non-permanent since the withdrawal of ALO causes the reappearance of the aneurysm; (vi) ALO inhibits redox stress-associated reactions such as the formation and accumulation of 3-NT, the nuclear translocation of pNRF2, and the collagen-associated fibrotic remodeling of the aortic media; and (vii) ALO also prevents the characteristic MFS endothelial-dependent vasodilator dysfunction. Mechanistically, ALO seems to mediate these effects by primarily reducing abnormally high H_2O_2 levels and associated redox stress injuries occurring in MFS aorta acting as a ROS scavenger. We here demonstrated ALO effectiveness

as an anti-redox stress drug, suggesting its potential repositioning use for preventing MFS aortopathy.

In MFS patients, XDH upregulation is favored towards the oxidase enzymatic form (XO). Interestingly, this is highly produced in the adjacent non-dilated zone of the aortic aneurysm. It is likely that in the dilated zone, where the histological damage is much more severe, the characteristic loss of VSMC explains the lesser expression observed. Notice that in the dilated zone, despite the variability of results, there is also a reduction of the XDH form compared with the non-dilated area. Most likely, the XO upregulation in the non-dilated zone is more representative of the molecular aortic injuries than the dilated zone since the structural changes are on their way to being produced but are not so dramatic as in the dilated zone where the aortopathy is severe and irreversible.

XDH mRNA and protein expression levels, as well as XO enzymatic activity are significantly upregulated in MFS aortae in young (3-month-old) but not in older mice (6-month-old). It is possible that XDH upregulation only occurs while the aortic dilation undergoes rapid growth, which we observed occurs until 3 months of age, becoming slower in older animals *(45)*. However, no differences between WT and MFS aortae have been reported regarding XDH activity in the study context of the aortic reactivity of MFS aorta *(14)*, and of nitro-oleic acid as a mediator in ERK1/2 and NOS2 expression in MFS aortopathy *(65)*. Explanations for this apparent discrepancy may be related to the different murine MFS models used (mgR/mgR and AngII infusion-induced acceleration of the aortopathy in MFS mouse, respectively) or the different XDH activity assays utilized, and/or even to local animal facility conditions.

We previously demonstrated the contribution of NOX4 in the progression of aortic aneurysm *(17)*, but its precise role in the aortopathy was not assayed due to the absence of a well-established selective inhibitor. Fortunately, this is not the case for XDH, with ALO being a well characterized specific inhibitor *(48)*. The clinical actions of ALO are widely linked to UA-associated pathologies *(66, 67)*. Nonetheless, ALO's mechanism of action also involves a concomitant reduction of ROS and, therefore, of oxidative stress, and, in the end, these two effects can probably explain most of its clinical efficacy. Strikingly, UA plasma levels in MFS mice were indistinguishable from those of WT, which was confirmed when we analyzed the plasma levels of allantoin and the resulting unchanged ratio. Plasma UA levels in ALO-treated mice were found to be unchanged, which discard a UA-mediated effect in the blocking of aortic dilation progression after ALO treatment. Both observations are demonstrative that the inhibitory effect of ALO in the aortopathy is not primary mediated through UA. Nonetheless, we cannot discard that lowering UA from normal baseline levels, the interference from other metabolic pathways, or using other XDH inhibitors (for example, febuxostat) might also contribute to protection against redox stress.

It has been reported that ALO has a direct intrinsic scavenger effect on ROS, regardless of its XDH activity inhibition *(68–70)*. When we tested this possibility by measuring ROS (H_2O_2) production in freshly dissected ascending aortic rings where local aerobic and pH conditions favor XDH for H_2O_2 production, ALO prevented its overproduction. At the same time, characteristic pathological processes that usually accompany redox stress, such as the formation of 3-NT, pNRF2 nuclear translocation, and fibrotic remodeling responses were reduced or fully inhibited. The pathophysiological significance of these latter results in the MFS aortic media

suggests several conclusions: (i) the accumulation of 3-NT is representative of abnormal RNS formation because of the pathological uncoupling of NO, which in turn leads to protein nitration via the formation of the highly reactive intermediate peroxynitrite and its subsequent product 3-NT *(71)*. This 3-NT upsurge in MFS aortic media is consistent with the recent demonstration of NO uncoupling in aneurysm formation in both MFS mice and patients *(65, 72, 73)*. Along this line of evidence, we previously identified actin as a significant nitrated protein target in MFS aorta from MFS patients *(17)*, contributing in this manner to the reported damaged contractile properties of VSMC in MFS *(74)*; (ii) redox stress is so elevated in MFS aorta that the intrinsic physiological antioxidant response mediated by the nuclear translocation of pNRF2 *(56)* is not high enough to compensate it. In contrast, ALO treatment allows this compensation, normalizing, to a large extent, the endogenous redox levels in MFS aorta and reverting the subsequent redox stress modifications; and (iii) the excessive accumulation of collagen (vascular fibrosis) and proteoglycans is characteristic of the aortic wall to compensate elastic fiber disarray *(75)*. In fact, this is the trend that we observe in the MFS media, where immature (green) collagen fibers are increased. ALO normalized, to a good extent, the content of green fibers, hence mitigating the fibrotic remodeling response that usually accompanies the aneurysm. It would be interesting to know whether ALO is also able to prevent the characteristic phenotypic switch of VSMC to a mixed contractile-secretory phenotype *(75, 76)*, where besides a variety of contractile markers, the expression of *COLα1* is enhanced and could, therefore, explain the abnormal expression and assembly of collagen fibers observed here.

An abnormally high XO-associated endothelium interaction most likely increases local ROS rates, leading to endothelial dysfunctions *(77)*. We report that XDH is immunolocalized to the intima and media aortic layers of WT mice, both being overexpressed in MFS animals. We think that the increased XDH localization in the MFS intima favors the local increase of 3-NT, which in turn is related to endothelial dysfunction. Note that ALO normalized ACh-stimulated vasodilator function and it is no surprise that ALO is responsible for the improvement in endothelial function given its reported effects on increasing NO bioavailability, attributable, at least in part, to a reduction in ROS production. Strikingly, the addition of unspecific NO donor NTP, an endothelium-independent relaxant agent, induced similar vasodilation in WT and MFS aortae, suggesting that the VSMC-associated NO/sGC/cGMP pathway is not altered. This result is seemingly in contrast to recently reported evidence using the same MFS mouse model, where an increase in plasma cGMP levels was reported *(73)*. It is possible that the different age of the mice used in both studies may explain the difference and/or circulating cGMP appears not to be a consistently good indicator of sGC activity in MFS ascending aorta. Further studies are needed to clarify this point.

One other potential and complementary mechanism by which ALO reduces aortic wall disarray is through XDH-derived ROS activation of MPPs, since ROS are potent activators of MMPs *(78)*. MMP2 and MMP9, two well-known MMPs involved in MFS aortopathy *(79)*, can be indirectly activated by ROS from their inactive-zymogen isoforms as well as via activation of their gene expression *(80)*. Likewise, it has been also reported that XDH itself can directly activate MMPs in a ROS-independent manner *(81)*. It cannot be discarded that ALO also mediates other XDH-independent

actions such as the inhibition of heat shock protein expression *(82)*, considering its significant role in MFS *(83)*.

We are aware that our study has some limitations: (i) ALO has a short half-life in plasma and is rapidly metabolized to oxypurinol, which has a longer lifespan *(48)*. It is possible that oxypurinol rather than allopurinol might be the primary metabolite that directly mediates the results we report here; (ii) the MFS model used in our study (C1041G) is a very useful model to evaluate the temporal course of aortopathy (besides other clinical manifestations), but it is not the most suitable to evaluate the survival rate after ALO treatments. Other more severe MFS murine models for aortic dissection and rupture, such as the *Fbn1* hypomorphic mouse (mgR/mgR) *(84)* or the AngII-induced accelerated model of MFS aortopathy *(65)*, both leading to aortic dissection and rupture, should be more appropriate experimental murine models for this aim; and (iii) we have only studied ALO's effects on the cardiovascular system (TAA more specifically), because it is responsible for the most life-threatening complications. Nevertheless, since MFS is a multisystemic disorder, it would also be of interest to study the putative effects of ALO on the other systems affected, even though it has been shown to be a safe and well-tolerated drug.

In conclusion, our results place redox stress among the molecular mechanisms that actively participate in the pathogenesis of aortic aneurysm in MFS by the consistent overproduction of ROS mediated by the overexpression of XDH (current study), the NADPH oxidases NOX4 *(17)* and NOX2 *(65)*, the severe dysfunction of NOS *(72)*, and mitochondria-associated redox stress *(85)*, all being studies performed both in MFS murine models and patients. How, and to what extent, do each of these interlinked mechanisms participate in the aortic injury is currently unknown, but most

likely they all act additively or synergistically to damage the aorta severely and permanently. Our results support the design of clinical trials based on well-characterized redox stress inhibitors, such as we report here for ALO. Importantly, ALO is a cheap drug, which is widely prescribed in clinical practice since the latter half of the last century and, most importantly, is proven to be effective, safe, and well tolerated. Finally, results in mice indicate that the potential beneficial effect of ALO in MFS patients could only be obtained whether the drug is administrated chronically.

METHODS

A study design scheme is shown in Fig. S2.

All Methods and Study approval declaration are in Supplementary Materials.

SUPPLEMENTARY MATERIAL

Complete Methods section.

Fig. S1. Reference positive control assay for the XO and XDH enzymatic activities performed in liver lysates.

Fig. S2. Representative scheme of the followed experimental protocols for allopurinol treatments.

Fig. S3. Aortic root diameter following allopurinol withdrawal.

Fig. S4. Uric acid and allantoin blood plasma levels are not altered in MFS mice.

Fig. S5. Allopurinol does not alter systolic blood pressure.

Fig. S6. XDH protein levels are not affected by allopurinol treatments.

Fig. S7. H_2O_2 plasma levels do not change with age in MFS mice.

Fig. S8. *In vitro* treatment of allopurinol reduces the formation of H_2O_2 in the ascending aorta of young MFS mice.

Fig. S9. Preventive treatment with allopurinol does affect the collagen content and its maturation state in the media of MFS mice.

Fig. S10. Aortic root diameter measured by ultrasonography of 9-month-old WT and MFS mice palliatively treated or not with allopurinol for 28 weeks (PA2).

Table S1. Primers used in RT-PCR analysis in MFS mice.

Table S2. Aortic root diameter (in mm) of WT and MFS mice subjected to palliative treatment (PA1) with allopurinol.

Table S3. Aortic root diameter (in mm) of WT and MFS mice subjected to preventive treatment (PE) with allopurinol.

Table S4. Aortic root diameter (in mm) of WT and MFS subjected to preventive allopurinol treatment (PE) and the subsequently drug withdrawal (PE-ALO).

Table S5. Aortic root diameter (in mm) of WT and MFS mice subjected to palliative treatment (PA2) with allopurinol.

Table S6. Potency (pEC50) and maximum response (Emax) of the concentration-response curves values for ACh- and NTP-induced relaxation response (%) in the ascending aorta in the presence or absence of allopurinol.

Table S7. KCl vascular tone, potency, and maximum response of the concentration–response curve values for the Phe-induced contraction response in the ascending aorta in the presence or absence of allopurinol.

Author contributions

Conceptualization: GE; Methodology: IR-R, KdR, CA, BP, AC, MA, FJ-A. Investigation: IR-R, KdR, CA, BP, MA, VC, FJ-A, GE; Funding acquisition: GE, FJ-

A and MCG-C; Supervision: GT-T, MCG-C, VC, FJ-A, GE; Writing – original draft: GE; Writing – review & editing: all authors.

The manuscript shares 3 co-first authorship, whose specific order was assigned and agreed considering the best chances to get as soon as possible the Ph.D. for IR-R, as well as a Ph.D. fellowship and a postdoctoral contract abroad for KdeR and CA, respectively. They have been aware of this co-first authorship explanation.

Acknowledgements

This work has been funded by a poorly endowed Spanish Ministry of Innovation and Science government grant PID2020-113634RB-C2 to GE and FJ-A, and a Spanish Ministry of Innovation and Science government grant PID2019-110906RB-I00 from to MCG-C. We thank Isabel Fabregat and Hal Dietz for critically reading the manuscript, Ana Paula Dantas (IDIBAPS) and Coral Sanfeliu (CSIC) for helpful methodological advice with H_2O_2 fluorometric measurements, Helena Kruyer for editorial assistance and Maite Muñoz for lab management.

REFERENCES

1. Dietz HC, et al. Marfan syndrome caused by a recurrent de novo missense mutation in the fibrillin gene. *Nature*. 1991;352(6333):337-339.
2. Keane MG, Pyeritz RE. Medical management of Marfan syndrome. *Circulation*. 2008;117(21):2802-2813.
3. Costa TJ, et al. The homeostatic role of hydrogen peroxide, superoxide anion and nitric oxide in the vasculature. *Free Radic Biol Med*. 2021;162:615-635.

4. Chen Q, et al. Reactive oxygen species: Key regulators in vascular health and diseases. *Br J Pharmacol*. 2018;175(8):1279-1292.

5. Miller FJ, et al. Oxidative stress in human abdominal aortic aneurysms: A potential mediator of aneurysmal remodeling. *Arterioscler Thromb Vasc Biol*. 2002;22(4):560-565.

6. McCormick ML, et al. Role of oxidative stress in the pathogenesis of abdominal aortic aneurysms. *Arterioscler Thromb Vasc Biol*. 2007;27(3):461-469.

7. Papalambros E, et al. Malondialdehyde as an indicator of oxidative stress during abdominal aortic aneurysm repair. *Angiology*. 2007;58(4):477-482.

8. Xiong W, et al. Inhibition of reactive oxygen species attenuates aneurysm formation in a murine model. *Atherosclerosis*. 2009;202(1):128-134.

9. Aivatidi C, et al. Oxidative stress during abdominal aortic aneurysm repair--biomarkers and antioxidant's protective effect: A review. *Eur Rev Med Pharmacol Sci*. 2011;15(3):245-252.

10. Pincemail J, et al. On the potential increase of the oxidative stress status in patients with abdominal aortic aneurysm. *Redox Rep*. 2012;17(4):139-144.

11. Portelli SS, et al. Oxidative stress in genetically triggered thoracic aortic aneurysm: Role in pathogenesis and therapeutic opportunities. *Redox Rep*. 2021;26(1):45-52.

12. Ejiri J, et al. Oxidative stress in the pathogenesis of thoracic aortic aneurysm: Protective role of statin and angiotensin II type 1 receptor blocker. *Cardiovasc Res*. 2003; 59(4):988-996.

13. Fiorillo C, et al. Evidence for oxidative stress in plasma of patients with Marfan syndrome. *Int J Cardiol*. 2010;145(3):544-546.

14. Yang HH, et al. Vasomotor dysfunction in the thoracic aorta of Marfan syndrome is associated with accumulation of oxidative stress. *Vascul Pharmacol*. 2010;52(1-2):37-45.

15. Branchetti E, et al. Oxidative stress modulates vascular smooth muscle cell phenotype via CTGF in thoracic aortic aneurysm. *Cardiovasc Res*. 2013;100(2):316-324.

16. Zúñiga-Muñoz AM, et al. Glutathione system participation in thoracic aneurysms from patients with Marfan syndrome. *Vasa*. 2017; 46(3):177-186.

17. Jiménez-Altayó F, et al. Redox stress in Marfan syndrome: Dissecting the role of the NADPH oxidase NOX4 in aortic aneurysm. *Free Radic Biol Med*. 2018;118:44-58.

18. Emrich F, et al. Anatomically specific reactive oxygen species production participates in Marfan syndrome aneurysm formation. *J Cell Mol Med*. 2019;23(10):7000-7009.

19. Egea G, et al. Reactive oxygen species and oxidative stress in the pathogenesis and progression of genetic diseases of the connective tissue. *Antioxidants (Basel)*. 2020;9(10):2013.

20. Rysz J, et al. Oxidative stress-related susceptibility to aneurysm in Marfan's syndrome. *Biomedicines*. 2021;9(9):1171.

21. Boueiz A, et al. Xanthine oxidoreductase in respiratory and cardiovascular disorders. *Am J Physiol Lung Cell Mol Physiol*. 2008;294(5):L830-840.

22. McManaman JL, Bain DL. Structural and conformational analysis of the oxidase to dehydrogenase conversion of xanthine oxidoreductase. *J Biol Chem*. 2002;277(24):21261-21268.

23. Lacy F, et al. Role of xanthine oxidase in hydrogen peroxide production. *Free Radic Biol Med*. 1998;25(6):720-727.

24. Cantu-Medellin N, Kelley EE. Xanthine oxidoreductase-catalyzed reactive species generation: A process in critical need of reevaluation. *Redox Biol*. 2013;1(1):353-358.

25. Schmidt HM, et al. The impact of xanthine oxidase (XO) on hemolytic diseases. *Redox Biol*. 2019;21:101072.

26. Yang HH, et al. Long-term effects of losartan on structure and function of the thoracic aorta in a mouse model of Marfan syndrome. *Br J Pharmacol*. 2009;158(6):1503-1512.

27. Soto ME, et al. Oxidant/antioxidant profile in the thoracic aneurysm of patients with the Loeys-Dietz syndrome. *Oxid Med Cell Longev*. 2020;2020:5392454.

28. Maiuolo J, et al. Regulation of uric acid metabolism and excretion. *Int J Cardiol*. 2016;213:8-14.

29. Doehner W, et al. Effects of xanthine oxidase inhibition with allopurinol on endothelial function and peripheral blood flow in hyperuricemic patients with chronic heart failure: Results from 2 placebo-controlled studies. *Circulation*. 2002;105(22):2619-2624.

30. Kand'ár R, et al. Monitoring of antioxidant properties of uric acid in humans for a consideration measuring of levels of allantoin in plasma by liquid chromatography. *Clin Chim Acta*. 2006;365(1-2):249-256.

31. Kanbay M, et al. The role of uric acid in the pathogenesis of human cardiovascular disease. *Heart*. 2013;99(11):759-766.

32. Vassalle C, et al. Uric acid for cardiovascular risk: Dr. Jekyll or Mr. Hide? *Diseases*. 2016;4(1):12.

33. Glantzounis GK, et al. Uric acid and oxidative stress. *Curr Pharm Des*. 2005;11(32):4145-4151.

34. Kang DH, Ha SK. Uric acid puzzle: Dual role as anti-oxidant and pro-oxidant. *Electrolyte Blood Press*. 2014;12(1):1-6.

35. Corry DB, et al. Uric acid stimulates vascular smooth muscle cell proliferation and oxidative stress via the vascular renin-angiotensin system. *J Hypertens*. 2008;26(2):269-275.

36. Yu MA, et al. Oxidative stress with an activation of the renin-angiotensin system in human vascular endothelial cells as a novel mechanism of uric acid-induced endothelial dysfunction. *J Hypertens*. 2010;28(6):1234-1242.

37. Patetsios P, et al. Identification of uric acid in aortic aneurysms and atherosclerotic artery. *Ann N Y Acad Sci*. 1996;800:243-245.

38. Esen AM, et al. Uric acid as a marker of oxidative stress in dilatation of the ascending aorta. *Am J Hypertens*. 2011;24(2):149-154.

39. Jiang WL, et al. Serum uric acid is associated with aortic dissection in Chinese men. *Int J Cardiol*. 2016;202:196-197.

40. Houston M, et al. Xanthine oxidase reaction with nitric oxide and peroxynitrite. *Arch Biochem Biophys*. 1998;355(1):1-8.

41. Ischiropoulos H. Biological tyrosine nitration: A pathophysiological function of nitric oxide and reactive oxygen species. *Arch Biochem Biophys*. 1998;356(1):1-11.

42. Ndrepepa G. Uric acid and cardiovascular disease. *Clin Chim Acta*. 2018;484:150-163.

43. Huang K, et al. Targeting feed-forward signaling of TGFβ/NOX4/DHFR/eNOS uncoupling/TGFβ axis with anti-TGFβ and folic acid attenuates formation of aortic aneurysms: Novel mechanisms and therapeutics. *Redox Biol*. 2021;38:101757.

44. Kelkar A, et al. Allopurinol as a cardiovascular drug. *Cardiol Rev*. 2011;19(6):265-271.

45. Arce C, et al. Anti-TGFβ (transforming growth factor β) therapy with betaglycan-derived P144 peptide gene delivery prevents the formation of aortic aneurysm in a mouse model of Marfan syndrome. *Arterioscler Thromb Vasc Biol*. 2021;41(9):e440-e452.

46. Amaya Y, et al. Proteolytic conversion of xanthine dehydrogenase from the NAD-dependent type to the O2-dependent type. Amino acid sequence of rat liver xanthine dehydrogenase and identification of the cleavage sites of the enzyme protein during irreversible conversion by trypsin. *J Biol Chem*. 1990;265(24):14170-14175

47. Beckman JS, et al. A sensitive fluorometric assay for measuring xanthine dehydrogenase and oxidase in tissues. *Free Radic Biol Med*. 1989;6(6):607-615.

48. Day RO, et al. Clinical pharmacokinetics and pharmacodynamics of allopurinol and oxypurinol. *Clin Pharmacokinet*. 2007;46(8):623-644.

49. Masaoka N, et al. Transplacental effects of allopurinol on suppression of oxygen free radical production in chronically instrumented fetal lamb brains during

intermittent umbilical cord occlusion. *J Matern Fetal Neonatal Med*. 2005;18(1):1-7.

50. Torrance HL, et al. Maternal allopurinol during fetal hypoxia lowers cord blood levels of the brain injury marker S-100B. *Pediatrics*. 2009;124(1):350-357.
51. Derks JB, et al. Allopurinol reduces oxidative stress in the ovine fetal cardiovascular system after repeated episodes of ischemia-reperfusion. *Pediatr Res*. 2010;68(5):374-380.
52. Niu Y, et al. Maternal allopurinol prevents cardiac dysfunction in adult male offspring programmed by chronic hypoxia during pregnancy. *Hypertension*. 2018;72(4):971-978.
53. Chung HY, et al. Xanthine dehydrogenase/xanthine oxidase and oxidative stress. *Age (Omaha)*. 1997;20(3):127-140.
54. Hille R, Massey V. Studies on the oxidative half-reaction of xanthine oxidase. *J Biol Chem*. 1981;256(17):9090-9095.
55. Kelley EE, et al. Hydrogen peroxide is the major oxidant product of xanthine oxidase. *Free Radic Biol Med*. 2010;48(4):493-498.
56. Ma Q. Role of Nrf2 in oxidative stress and toxicity. *Annu Rev Pharmacol Toxicol*. 2013;53:401-426.
57. Lindeman JH, et al. Distinct defects in collagen microarchitecture underlie vessel-wall failure in advanced abdominal aneurysms and aneurysms in Marfan syndrome. *Proc Natl Acad Sci USA*. 2010;107(2):862-865.
58. Busnadiego O, et al. Elevated expression levels of lysyl oxidases protect against aortic aneurysm progression in Marfan syndrome. *J Mol Cell Cardiol*. 2015;85:48-57.

59. López-Guimet J, et al. MicroCT imaging reveals differential 3D micro-scale remodelling of the murine aorta in ageing and Marfan syndrome. *Theranostics*. 2018;8(21):6038-6052.

60. Rittié L. Method for picrosirius red-polarization detection of collagen fibers in tissue sections. *Methods Mol Biol*. 2017;1627:395-407.

61. Kelley EE. A new paradigm for XOR-catalyzed reactive species generation in the endothelium. *Pharmacol Rep*. 2015;67(4):669-674.

62. Chung AW, et al. Endothelial dysfunction and compromised eNOS/Akt signaling in the thoracic aorta during the progression of Marfan syndrome. *Br J Pharmacol*. 2007;150(8):1075-1083.

63. Jiménez-Altayó F, et al. Differences in the thoracic aorta by region and sex in a murine model of Marfan syndrome. *Front Physiol*. 2017;8:933.

64. Kocyigit D, et al. Medical therapies for Marfan syndrome and other thoracic aortic dilatation in adults: A contemporary review. *Am J Cardiovasc Drugs*. 2021;21(6):609-617.

65. Nettersheim FS, et al. Nitro-oleic acid (NO2-OA) reduces thoracic aortic aneurysm progression in a mouse model of Marfan syndrome. *Cardiovasc Res*. 2021;cvab256.

66. Chen C, et al. Hyperuricemia-related diseases and xanthine oxidoreductase (XOR) inhibitors: An overview. *Med Sci Monit*. 2016;22:2501-2512.

67. Bove M, et al. An evidence-based review on urate-lowering treatments: Implications for optimal treatment of chronic hyperuricemia. *Vasc Health Risk Manag*. 2017;13:23-28.

68. Das DK, et al. Role of xanthine oxidase inhibitor as free radical scavenger: A novel mechanism of action of allopurinol and oxypurinol in myocardial salvage. *Biochem Biophys Res Commun*. 1987;148(1):314-319.

69. George J, Struthers AD. Role of urate, xanthine oxidase and the effects of allopurinol in vascular oxidative stress. *Vasc Health Risk Manag*. 2009;5(1):265-272.

70. Nogueira RC, et al. Omeprazole induces vascular remodeling by mechanisms involving xanthine oxidoreductase and matrix metalloproteinase activation. *Biochem Pharmacol*. 2021;190:114633.

71. Radi R. Protein tyrosine nitration: Biochemical mechanisms and structural basis of functional effects. *Acc Chem Res*. 2013;46(2):550-559.

72. Oller J, et al. Nitric oxide mediates aortic disease in mice deficient in the metalloprotease Adamts1 and in a mouse model of Marfan syndrome. *Nat Med*. 2017; 23(2):200-212.

73. de la Fuente-Alonso A, et al. Aortic disease in Marfan syndrome is caused by overactivation of sGC-PRKG signaling by NO. *Nat Commun*. 2021;12(1):2628.

74. Milewicz DM, et al. Genetic basis of thoracic aortic aneurysms and dissections: Focus on smooth muscle cell contractile dysfunction. *Annu Rev Genomics Hum Genet*. 2008;9:283-302.

75. Pedroza AJ, et al. Single-cell transcriptomic profiling of vascular smooth muscle cell phenotype modulation in Marfan syndrome aortic aneurysm. *Arterioscler Thromb Vasc Biol*. 2020; 40(9):2195-2211.

76. Crosas-Molist E, et al. Vascular smooth muscle cell phenotypic changes in patients with Marfan syndrome. *Arterioscler Thromb Vasc Biol*. 2015;35(4):960-972.

77. Battelli MG, et al. Xanthine oxidoreductase-derived reactive species: Physiological and pathological effects. *Oxid Med Cell Longev*. 2016;2016:3527579.

78. Martinez-Lemus LA, Galiñanes EL. Matrix metalloproteinases and small artery remodeling. *Drug Discov Today Dis Models*. 2011;8(1):21-28.

79. Tehrani AY, et al. Characterization of doxycycline-mediated inhibition of Marfan syndrome-associated aortic dilation by multiphoton microscopy. *Sci Rep*. 2020;10(1):7154.

80. Valentin F, et al. Oxidative stress activates MMP-2 in cultured human coronary smooth muscle cells. *Fundam Clin Pharmacol*. 2005;19(6):661-667.

81. Liu W, et al. Xanthine oxidase activates pro-matrix metalloproteinase-2 in cultured rat vascular smooth muscle cells through non-free radical mechanisms. *Arch Biochem Biophys*. 2004;426(1):11-17.

82. Nishizawa J, et al. Reactive oxygen species play an important role in the activation of heat shock factor 1 in ischemic-reperfused heart. *Circulation*. 1999;99(7):934-941.

83. Siegert AM, et al. A FBN1 3'UTR mutation variant is associated with endoplasmic reticulum stress in aortic aneurysm in Marfan syndrome. *Biochim Biophys Acta Mol Basis Dis*. 2019;1865(1):107-114.

84. Pereira L, et al. Pathogenetic sequence for aneurysm revealed in mice underexpressing fibrillin-1. *Proc Natl Acad Sci U S A*. 1999;96(7):3819-3823.

85. Oller J, et al. Extracellular tuning of mitochondrial respiration leads to aortic aneurysm. *Circulation*. 2021;143(21):2091-2109.

86. Reagan-Shaw S, et al. Dose translation from animal to human studies revisited. *FASEB J*. 2008;22(3):659-661.

87. Kim KM, et al. A sensitive and specific liquid chromatography-tandem mass spectrometry method for the determination of intracellular and extracellular uric acid. *J Chromatogr B Analyt Technol Biomed Life Sci*. 2009;877(22):2032-2038.

88. El Mubarak MA, et al. Simultaneous determination of allantoin and glycolic acid in snail mucus and cosmetic creams with high performance liquid chromatography and ultraviolet detection. *J Chromatogr A*. 2013;1322:49-53.

89. Onetti Y, et al. Western-type diet induces senescence, modifies vascular function in non-senescence mice and triggers adaptive mechanisms in senescent ones. *Exp Gerontol*. 2013;48(12):1410-1419.

90. Rubies C, et al. Aortic remodelling induced by obstructive apneas is normalized with mesenchymal stem cells infusion. *Sci Rep*. 2019; 9(1):11443.

FIGURES WITH FIGURE LEGENDS

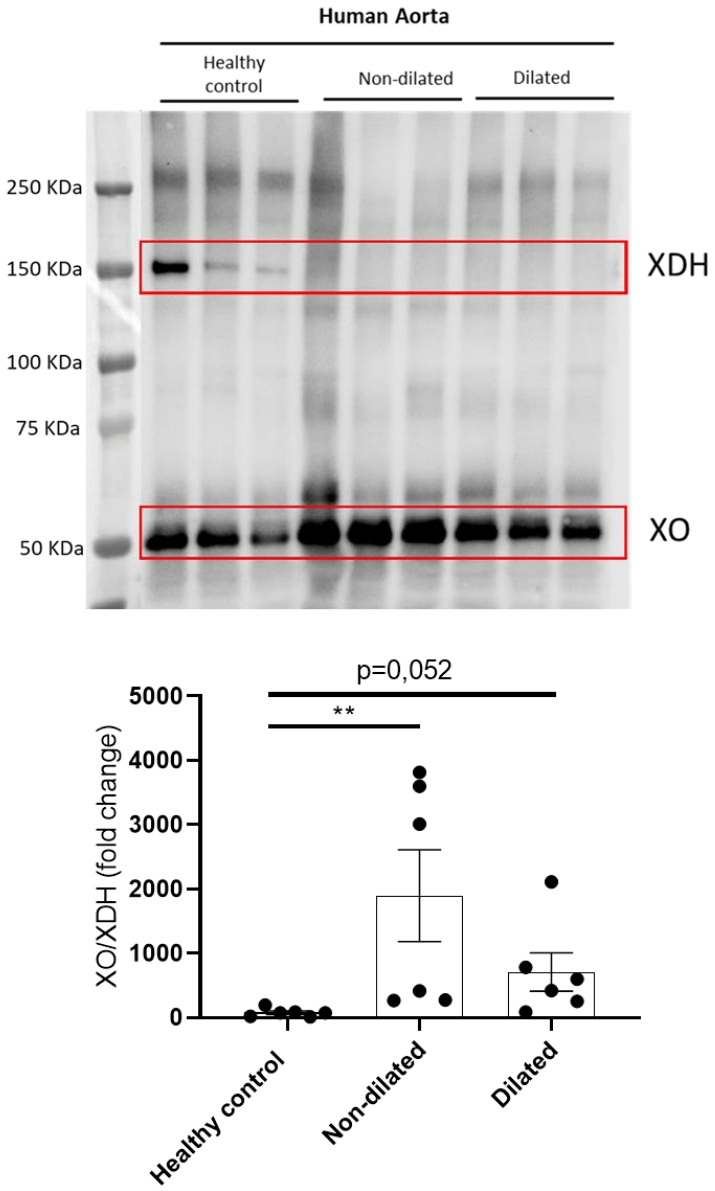

Figure 1. The Xanthine oxidase (XO) protein form is increased in the aortic aneurysm of MFS patients. XDH and XO protein forms of XDH/XOR revealed by western blotting in the dilated and adjacent non-dilated aneurysm zone of the aorta from Marfan patients subjected to aortic surgery and from healthy controls. The ratio between XO/XDH protein bands is shown below. Results are the mean ± SEM. Statistical test analysis: Kruskal-Wallis and Dunn´s post-test; ***P*≤0.01.

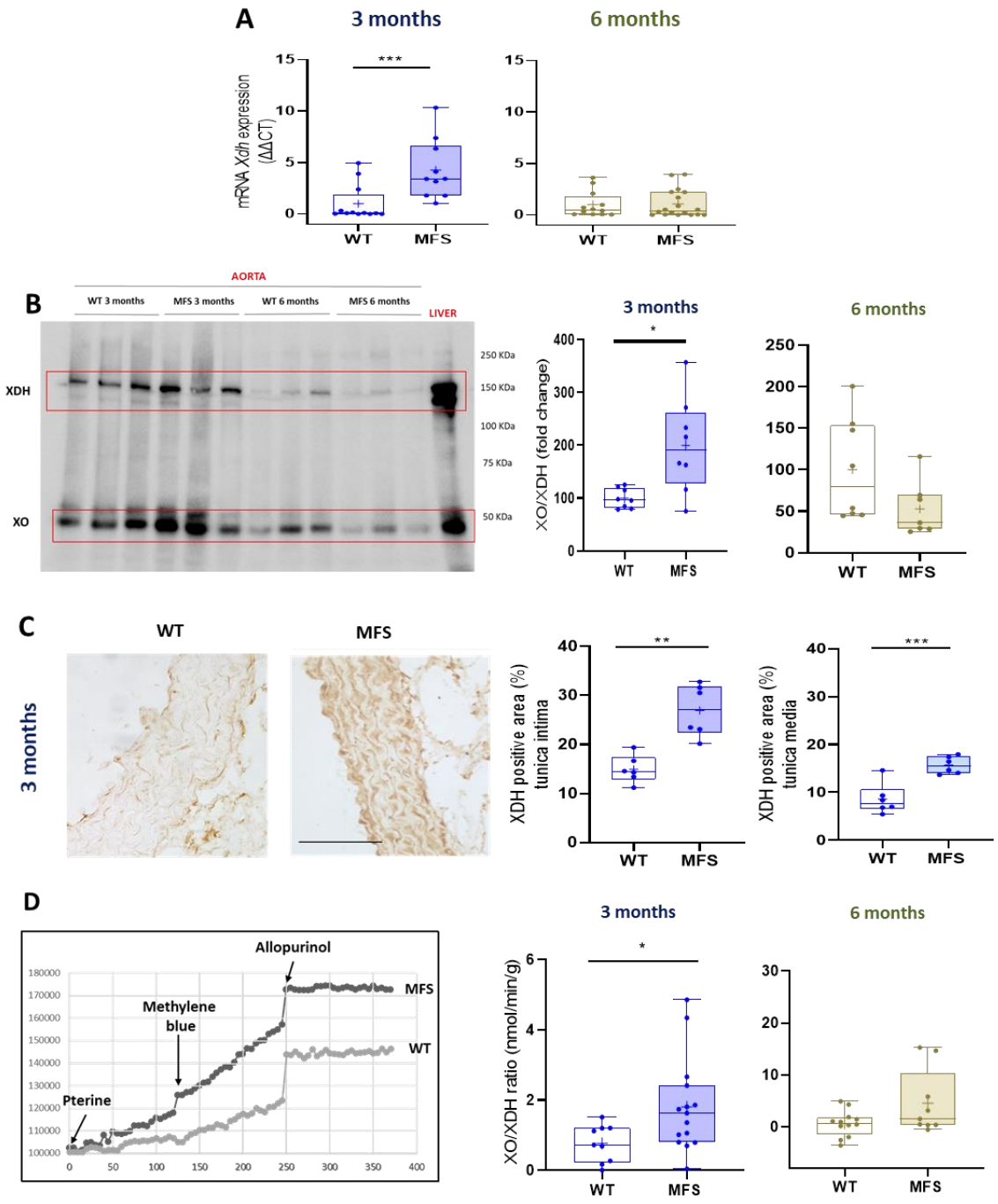

Figure 2. *XDH* mRNA expression levels, and XO protein formation and enzymatic activity are increased in MFS mice ascending aorta. **(A)** mRNA expression levels of XDH in WT and MFS mice of different ages (3 and 6 months-old; n=10-15). **(B)** XDH and XO protein bands revealed by western blotting in WT and MFS aorta of 3- and 6-month-old mice (n=7-8). The ratio between XO/XDH

protein bands is also shown. **(C)** XDH expression levels revealed by immunohistochemistry in paraffin-embedded aortae from 3-month-old WT and MFS mice (n=5). On the right, quantitative analysis of the respective HRP immunostaining in tunicae intima and media. Bar, 100 µm. **(D)** Representative assay for XO and XDH enzymatic activity forms (on the left) and the XO/XDH ratio in WT and 3- and 6-month-old MFS mice (on the right). A representative positive control assay performed in liver lysates is shown in Fig. S1. Data represented as boxplots. Statistical test analysis: Mann Whitney U test (A-D). ***$p \leq 0.001$, **$p \leq 0.01$, and *$p \leq 0.05$.

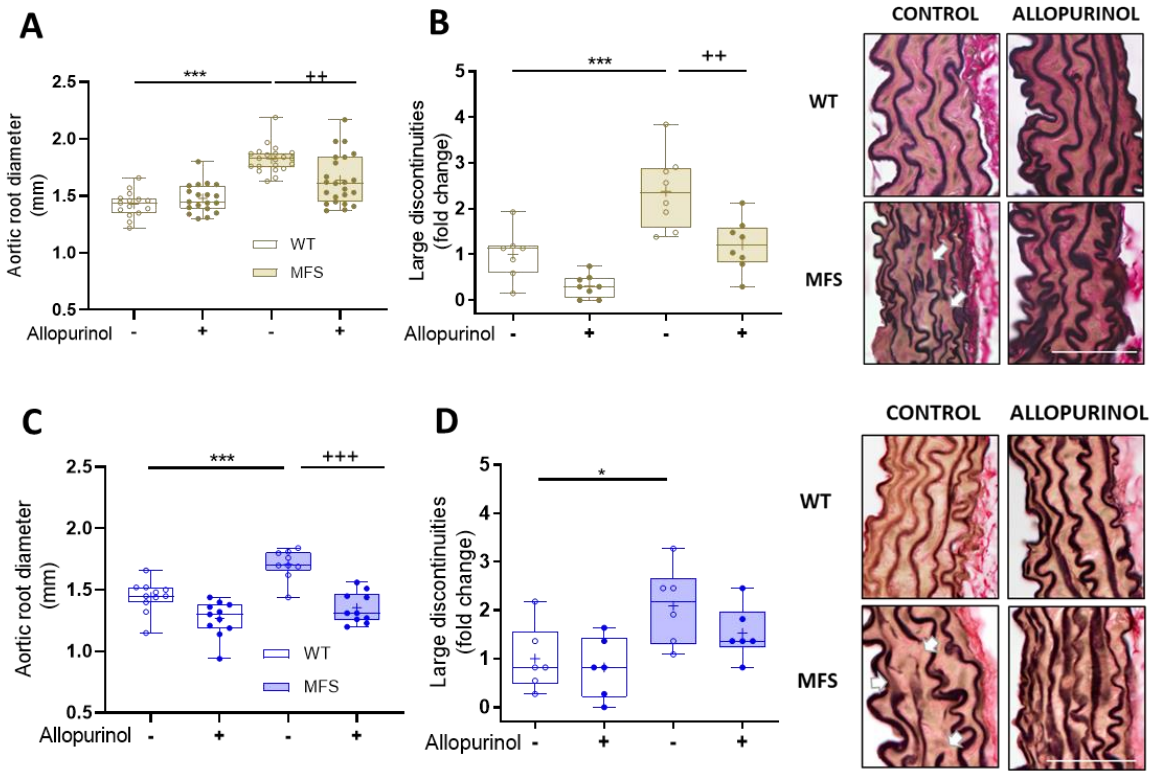

Figure 3. Allopurinol prevents the formation and progression of aortic root dilation in MFS mice. (A) Allopurinol halts the progression of aortic root dilatation in MFS mice measured by ultrasonography in WT and MFS mice of 6 months of age treated with allopurinol for 16 weeks (PA1). See also Table S2. (**B)** The number of large discontinuities in the elastic lamina of the aortic media (360º) from WT and MFS mice palliatively treated with allopurinol (n=14-16). **(C)** Allopurinol prevents the formation of aortic root dilatation in MFS mice measured by ultrasonography in 3-month-old WT and MFS mice preventively treated with allopurinol for 12 weeks (PE). See also Table S3. **(D)** Number of large discontinuities in the elastic lamina of the aortic media (360º) from WT and MFS mice preventively treated with allopurinol (n=9-11). On the right of panels B and D, representative Elastin Verhoeff-Van Gieson staining in paraffin sections of the ascending aorta. White arrows in B and D indicate examples of the large discontinuities analyzed. Bar, 100 µm. Data represented as boxplots. Statistical analysis: Two-way ANOVA and Tukey post-test (A and B). ***, $^{+++}P\leq0.001$, $^{++}P\leq0.01$ and $^{*}P\leq0.05$; *effect of genotype; $^{+}$effect of treatment.

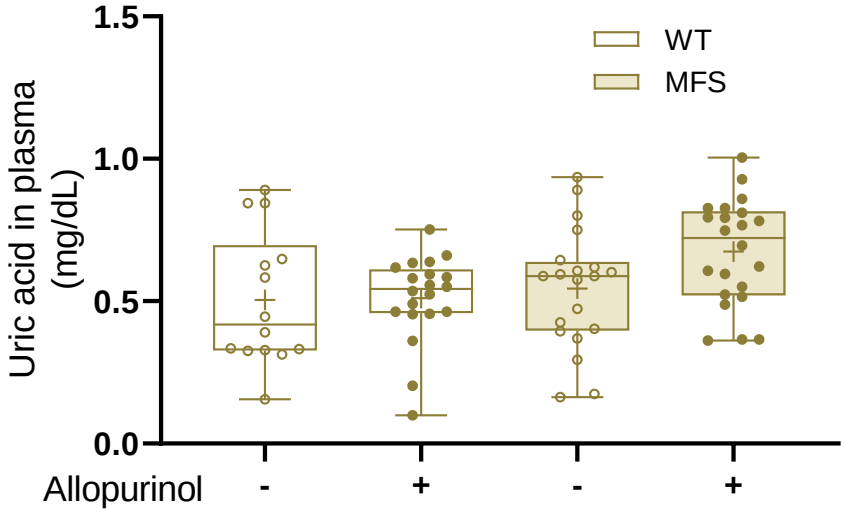

Figure 4. Allopurinol does not affect uric acid levels regardless of genotype. Uric acid blood plasma levels in WT and MFS mice palliatively treated or not with allopurinol for 16 weeks (PA1). Allopurinol does not affect UA plasma levels both in WT and MFS mice (n=14-22). Data represented as boxplots. Statistical analysis: Two-way ANOVA.

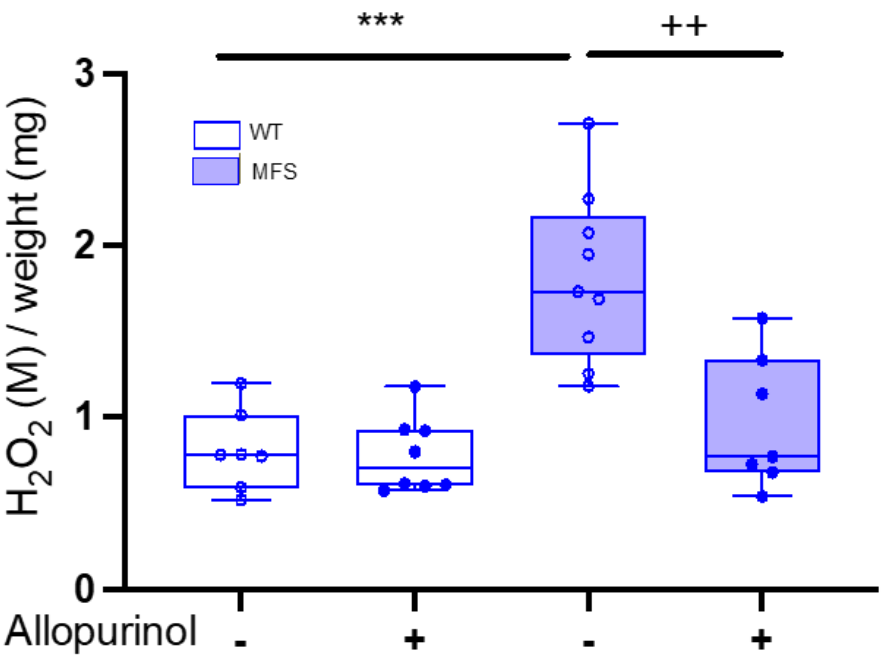

Figure 5. The overproduction of H_2O_2 in the ascending aorta of MFS mice is inhibited by the administration of allopurinol. Ascending aorta of WT and MFS mice (3 months-age) treated or not with allopurinol following the PE treatment were measured for the H_2O_2 production (n=6-9). Data represented as boxplots. Two-way ANOVA and Tukey's post-test. ***$P \leq 0.001$ and $^{++}P \leq 0.01$; *effect of genotype; $^{++}$effect of treatment.

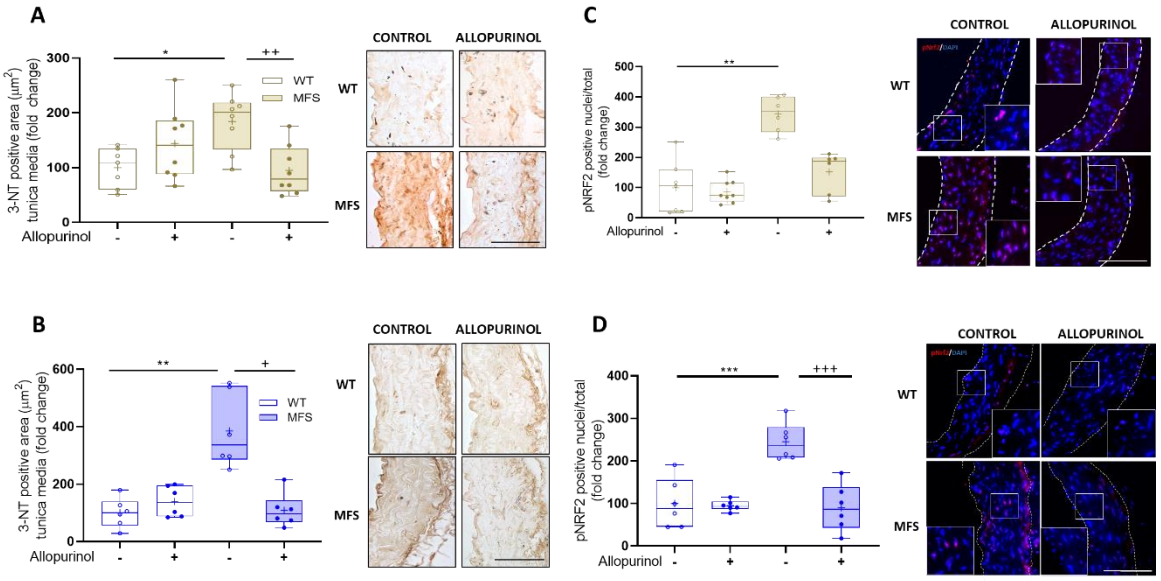

Figure 6. Allopurinol inhibits oxidative stress reactions occurring in the Marfan aortic media. **(A** and **B)** Quantitative analysis and representative images of the 3-NT levels in the aortic media evidenced by HRP immunohistochemistry after palliative (PA1; **A**) and preventive (PE; **B**) treatments with allopurinol in WT and MFS mice. Bar, 100 µm. **(C** and **D)** Quantitative analysis and representative images of the nuclear translocation of the phosphorylated form of NRF2 in VSMC of the tunica media of WT and MFS mice treated with allopurinol palliatively (PA1; **C**) and preventively (PE; **D**). Insets in the immunofluorescent images detail the nuclear localization of pNRF2. Bar, 100 µm. Data represented as boxplots. Statistical test: Two-way ANOVA and Tukey post-test (A); Kruskal-Wallis and Dunn's multiple comparison tests (B-D). $^{***,+++}P \leq 0.001$ $^{**,++}P \leq 0.01$ and $^{*,+}P \leq 0.05$; *effect of genotype; $^{+}$effect of treatment.

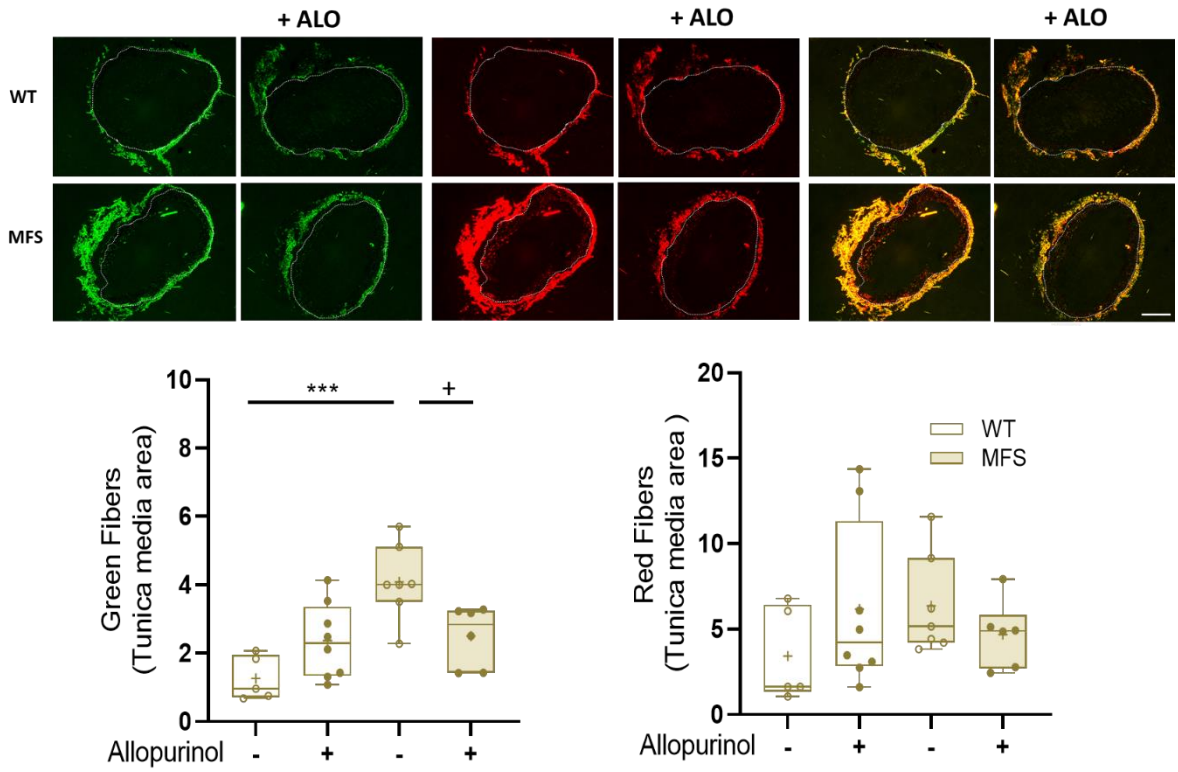

Figure 7. Palliative treatment with allopurinol reverts the MFS-associated fibrotic remodeling of the tunica media. Immature (green) and mature (red) collagen fibers of the tunicae media and adventitia of WT and MFS aortae stained with Picrosirius red visualized under the polarized microscope. WT and MFS mice treated or not with allopurinol in a palliative (PA1) manner (n=5-8). Representative fluorescent images of the whole aorta where white dashed lines display the limit between the tunicae media (inner) and adventitia (outer). Bar, 100 µm. The respective quantitative analysis of both types of collagen fibers is also shown. Data presented as boxplots. Statistical test: Kruskal-Wallis and Dunn's multiple comparison tests. ***$P \leq 0.001$ and $^{+}P \leq 0.05$; *effect of genotype; $^{+}$effect of treatment.

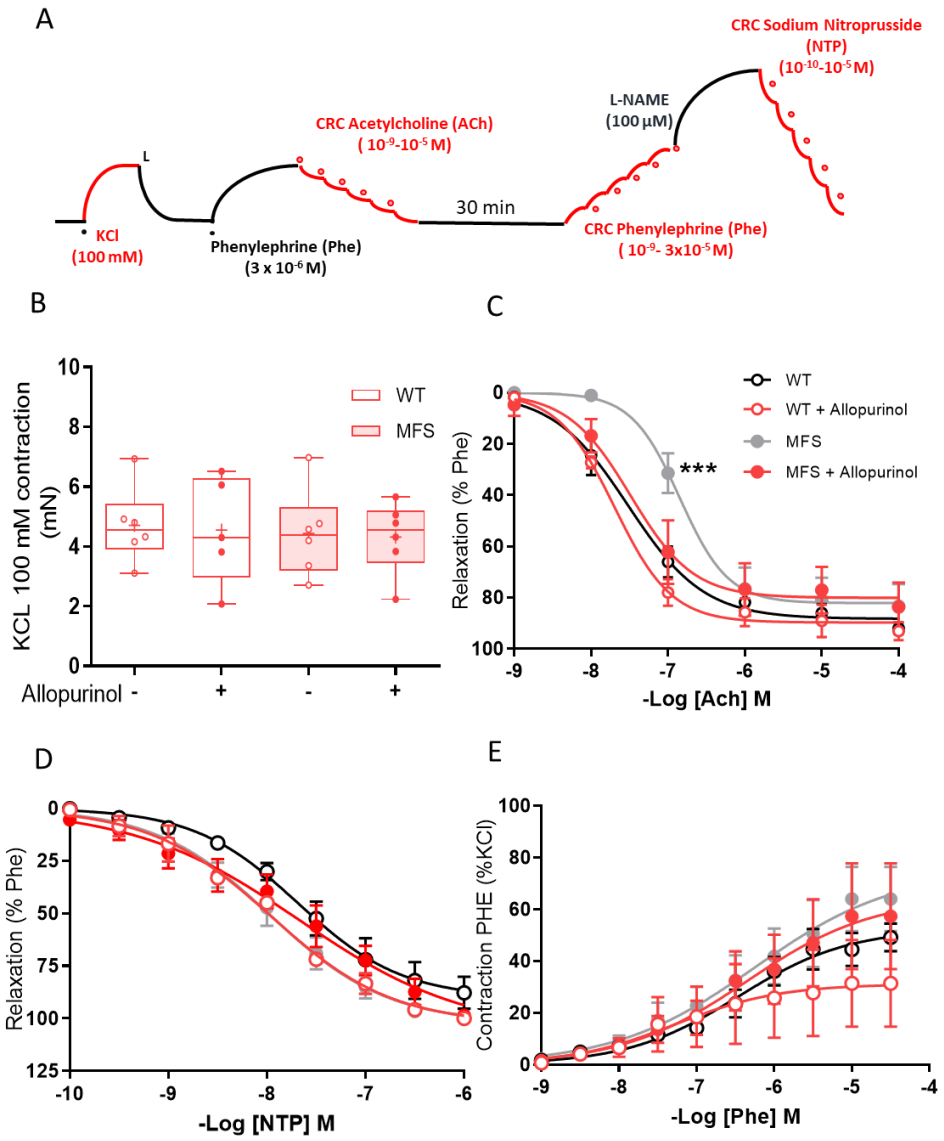

Figure 8. Allopurinol prevents the endothelial vasodilation dysfunction of MFS aorta. **(A)** Experimental protocol for the wire-myography experiments carried out in isolated 9-month-old ascending aorta of the diverse experimental groups indicated in the following panels. Red lines indicate where myographic measurements were obtained. **(B)** Physiological state test of aortic reactivity following the addition of KCl (100 mM). Data represented as boxplots. **(C)** Relaxation of aortic reactivity following ACh addition. **(D)** Relaxation reactivity after the addition of the NO donor sodium nitroprusside. **(E)** Contraction aortic reactivity after the addition of phenylephrine. Data in C-E are the mean ±SD. Statistical tests: Two-way ANOVA and Tukey post-test (B); non-liner regression of data by fitting Phe/ACh/NTP concentration-response curves to a sigmoidal dose response (C-E). ***$P \leq 0.001$.

SUPPLEMENTARY MATERIAL

ALLOPURINOL BLOCKS THE FORMATION AND PROGRESSION OF AORTIC ANEURYSM IN A MOUSE MODEL OF MARFAN SYNDROME

Isaac Rodríguez-Rovira[1,*], Karo de Rycke[1,*,¶], Cristina Arce[1,*,†], Belén Pérez[2], Aitor Carretero[3], Marc Arbonés[1], Gisela Teixidò-Turà[4], Mari Carmen Gómez-Cabrera[3], Victoria Campuzano[1,5], Francesc Jiménez-Altayó[2] and Gustavo Egea[1,#]

[1] Department of Biomedical Sciences, University of Barcelona School of Medicine and Health Sciences and IDIBAPS, 08036 Barcelona, Spain.

[2] Department of Pharmacology, Toxicology and Therapeutics, Neuroscience Institute, School of Medicine, Autonomous University of Barcelona, 08193 Cerdanyola del Vallès, Spain.

[3] Department of Physiology, Faculty of Medicine, University of Valencia, CIBERFES, Fundación Investigación Hospital Clínico Universitario/INCLIVA, Valencia, Spain.

[4] Department of Cardiology, Hospital Universitari Vall d'Hebron, Barcelona, Spain. CIBER-CV, Vall d'Hebron Institut de Recerca (VHIR), Barcelona, Spain

[5] Centro de Investigación Biomédica en Red de Enfermedades Raras (CIBERER), ISCIII, Spain.

[#] Corresponding author: Gustavo Egea, Dept. Biomedicina, Facultat de Medicina, Universitat de Barcelona, c/ Casanova 143, 08036 Barcelona, Spain, +34648557759, gegea@ub.edu

* These authors contributed equally to this work.

¶ Present address: Center for Medical Genetics, Department of Biomolecular Medicine, Ghent University, Ghent, 9000, Belgium.

† Present address: Dept of Biology, University of Padova, via Ugo Bassi 58b, Padova, Italy.

CONTENT

1. DETAILED METHODS. Pages: 2-13.

2. SUPPLEMENTAL FIGURES AND FIGURE LEGENDS). Pages: 14-23.

3. SUPPLEMENTAL TABLES. Pages: 24-27.

1. DETAILED METHODS

Human tissue collection, mice, and experimental designs

Healthy ascending aortic tissue was collected from heart donors via the organ donation organization at the Hospital Clínic i Provincial (Barcelona, Spain) and Hospital de Bellvitge, (L'Hospitalet de Llobregat, Barcelona, Spain). The age and gender of heart donors were unknown because Spanish law protects personal information about organ donors. Ascending aortic aneurysm samples were collected from MFS patients (with ages ranging from 23 to 59 years) undergoing aortic aneurysm repair surgery. All the patients in whom aortae were resected fulfilled Marfan diagnostic criteria according to Ghent nosology, but no genetic information regarding putative *FBN1* mutations was available. For each patient, we obtained a 3 x 3 cm sample from two areas: the dilated zone, corresponding to the sinuses of Valsalva, and the apparently adjacent virtually non-dilated aorta, corresponding to the distal ascending aorta. The aortae were maintained in cold saline solution or cardioprotective solution before delivery to the laboratory.

Marfan syndrome mice with fibrillin-1 mutation *(Fbn1*$^{C1041G/+}$*)* (hereafter, MFS mice) were purchased from The Jackson Laboratory (B6.129-Fbn1tm1Hcd/J; Strain #012885/Common name: C1039G; Bar Harbor, ME

04609, USA). MFS and sex- and age-matched wild-type littermates (WT mice) were maintained on a C57BL/6J genetic background. All mice were housed according to the University of Barcelona institutional guidelines (constant room temperature at 22ºC, controlled environment 12/12-hour light/dark cycle, 60% humidity and *ad libitum* access to food and water).

WT and MFS mice were administered allopurinol (hereafter ALO) (A8003, Sigma-Aldrich;) diluted in drinking water (20 mg/kg/day). The dose was calculated based on the human equivalent dose formula to convert the appropriate dose between species (86). ALO was fully replaced each third day of treatment. We performed two experimental ALO treatment approaches: palliative (PA) and preventive (PE). For PA treatments, ALO was administered to mice of 2 months of age until 6 or 9 months-old being a respective effective treatment of 16 and 28 weeks (named PA1 and PA2, respectively). For PE treatment, ALO was administered to the pregnant WT mother, maintained after giving birth (lactation period of 25 days) and thereafter maintained in drinking water to weaned babies until 3 months of age. In other PE experimental set, ALO was withdrawn from drinking water for the subsequent 3 months (PE-ALO; Fig. S2). At each outcome time points, mice were subjected to echocardiographic analysis, the liver and ascending aorta were dissected and fixed for paraffin embedding for (immuno)histological studies or immersed in RNA Later (R-0901, Sigma Aldrich), frozen in liquid nitrogen and stored at -80ºC for molecular tests.

Echocardiography

Two-dimensional transthoracic echocardiography was performed in all animals under 1.5% inhaled isoflurane. Each animal was scanned 12–24 hours

before sacrifice. Images were obtained with a 10–13 MHz phased array linear transducer (IL12i GE Healthcare, Madrid, Spain) in a Vivid Q system (GE Healthcare, Madrid, Spain). Images were recorded and later analyzed offline using commercially available software (EchoPac v.08.1.6, GE Healthcare, Madrid, Spain). Proximal aortic segments were assessed in a parasternal long-axis view. The aortic root diameter was measured from inner edge to inner edge in end-diastole at the level of the sinus of Valsalva. All echocardiographic measurements were carried out in a blinded manner by two independent investigators at two different periods, and with no knowledge of genotype and treatment.

Histology and histomorphometry

Paraffin-embedded tissue arrays of mice aortae from different experimental sets were cut into 5 µm sections. Elastic fiber ruptures were quantified by counting the number of large fiber breaks in tissue sections stained with Verhoeff-Van Gieson. Breaks larger than 20 µm were defined as evident large discontinuities in the normal circumferential continuity (360º) of each elastic lamina in the aortic media (45). They were counted along the length of each elastic lamina in four different, representative images of three non-consecutive sections of the same ascending aorta. All measurements were carried out in a blinded manner by two different observers with no knowledge of genotype and treatment. Images were captured using a Leica Leitz DMRB microscope (40x oil immersion objective) equipped with a Leica DC500 camera and analyzed with Fiji Image J Analysis software.

Immunohistochemistry and immunofluorescence staining

For immunohistochemistry and/or immunofluorescence, paraffin-embedded aortic tissue sections (5 µm thick) were deparaffinized and rehydrated prior to unmasking the epitope. Horse radish peroxidase (HRP)-based immunohistochemistry was used to stain aortic tissue sections for XDH and 3-nitrotyrosine (3-NT). To unmask XOR epitopes, aortic tissue sections were treated with a retrieval solution (10 mM sodium citrate, 0.05% Tween, pH 6) for 30 min in the steamer at 95ºC. No antigen retrieval was used for 3-NT. Next, sections were incubated for 10 min with peroxidase blocking solution (Dako Real Peroxidase-blocking solution; S202386-2), rinsed three times with PBS and then incubated with 1% BSA in PBS prior to overnight incubation at 4ºC with the respective primary polyclonal antibodies anti-XOR (1:50; Rockland 200-4183S) or anti-3-NT (1:200; Merck Millipore 06-284). On the next day, sections were incubated with the manufacturer's goat anti-rabbit secondary antibody solution (1:500; Abcam ab97051) for 1 h followed by the Liquid DAB+Substrate Chromogen System (Dako System HRP) for 1 min at room temperature. HRP-stained non-consecutive sections were visualized under a Leica Leitz DMRB microscope (40x immersion oil objective).

Immunofluorescence was used to stain pNrf2 in aortic sections. Sections were treated first with heat-mediated retrieval solution (1 M Tris-EDTA, 0.05% Tween, pH 9) for 30 min in the steamer at 95ºC. Next, sections were incubated for 20 minutes with ammonium chloride (NH_4Cl, 50 mM, pH 7.4) to block free aldehyde groups, followed by a permeabilization step using 0.3% Triton X-100 for 10 min and then treated with 1% BSA blocking buffer solution for 2 h prior to overnight incubation with monoclonal anti-pNRF2 (1:50; Abcam ab76026) in a

humidified chamber at 4°C. On the next day, sections were rinsed with PBS, followed by 60 min incubation with the secondary antibody goat anti-rabbit Alexa 647 (1:1.000, A-21246, Invitrogen). Sections were counterstained with DAPI (1:10.000) and images were acquired using an AF6000 widefield fluorescent microscope.

For quantitative analysis of immunostainings, four areas of each ascending aorta section were quantified with Image J software. All measurements were carried out in a blinded manner by two independent investigators.

Uric acid, allantoin and hydrogen peroxide measurements in blood plasma and/or ascending aortic rings

Whole blood from mice was collected directly from the left ventricle just before the aortic tissue was dissected. Thereafter, the blood plasma was obtained by centrifugation of unclotted blood at 3.000 rpm for 10 min at 4ºC and immediately stored frozen at -80 ºC.

Measurement of uric acid (UA) in blood plasma was evaluated by high-performance liquid chromatography (HPLC) with ultraviolet detection. The method used for UA extraction from biological samples was an adaptation of a method previously described (87). The plasma (100 µl) was deproteinized with 10% trichloroacetic acid. Ten µl of supernatant was injected into the HPLC system made up of a Perkin Elmer series 200 Pump, a 717 plus Auto sampler, a 2487 Dual λ absorbance detector, and a reverse-phase ODS2 column (Waters, Barcelona, Spain; 4.6 mm·200 mm, 5 µm particle size). The mobile phase was methanol/ammonium acetate 5 mM/acetonitrile (1:96:3 v/v), which was run with

an isocratic regular low flow rate of 1.2 mL/min and the wavelength UV detector was set at 292 nm. UA eluted at a retention time of 2.9 minutes. Quantification was performed by external calibration. The UA detection limit in plasma was 10 ng/mL

For the determination of allantoin in plasma, an adapted protocol was used as previously described (88). Briefly, plasma (60 µl) was deproteinized with acetonitrile (25 µl). Samples were centrifuged (5 min, 12,000*g*). Ten µl of supernatant was injected into the HPLC system. Separation of allantoin was performed on a Synergy Hydro-RP C-18 reversed-phase column (250 × 4.6 mm I.D., 5 m particle size) from Phenomenex (Torrance, CA, USA). Allantoin elution (at 4 min) was performed with potassium dihydrogen phosphate (10 mM, pH 2.7): acetonitrile (85:15) and ultraviolet detection (at 235 nm).

Hydrogen peroxide (H_2O_2) in plasma (50 µL) and dissected aortic tissue was determined utilizing a commercial assay kit (ab102500 Abcam, Cambridge, UK). In the case of aortic tissue, freshly dissected ascending aorta from 3-month-old WT and MFS mice subjected to PE treatment with ALO were isolated and quickly immersed in DMEM and incubated with OxiRed probe and HRP following the manufacturer's instructions. Measurements were obtained after 2 h. For *in vitro* treatment with ALO, 3- and 6-months-age aortic rings were divided in two equal portions along the proximal-distal heart axis. After a basal measurement, one of the two aortic portions were treated with allopurinol (100 µM, final concentration) while the other was treated with the vehicle (physiological serum/PS). Measurements were performed after 120 min. Results obtained following both *in vivo* and *in vitro* approaches were normalized by weight of the

respective aortic portion. Fluorescence was measured with a Synergy fluorimeter (Ex/Em = 535/587 nm).

Myography tissue preparation and vascular reactivity

Segments of the ascending aorta from 9-month-old mice treated or not with ALO were dissected free of fat and placed in a cold physiological salt solution (PSS; composition in mM: NaCl 112; KCl 4.7; $CaCl_2$ 2.5; KH_2PO_4 1.1; $MgSO_4$ 1.2; $NaHCO_3$ 25 and glucose 11.1) gassed with 95% O_2 and 5% CO_2. Ascending aortic segments (2-3 mm) were set up on an isometric wire myograph (model 410A; Danish Myo Technology, Aarhus, Denmark) filled with PSS (37ºC; 95% O_2 and 5% CO_2) as previously described (89). The vessels were stretched to 6 mN as reported (62), rinsed and allowed to equilibrate for 45 min. Tissues were then contracted twice with KCl (100 mM) every 5 min. After rinsing, vessels were left to equilibrate for an additional 30 min before starting the experiments. Vasodilatation caused by nitric oxide (NO) produced either by the endothelium itself (triggered by acetylcholine/ACh) or by the NO donor sodium nitroprusside (NTP) were determined by cumulative concentration-response curves (CRCs) of respective relaxation to ACh (10^{-9}-10^{-5} M) or NTP (10^{-10}-10^{-5} M) after phenylephrine (Phe; 3×10^{-6} M) induced precontracted vessel. To study the impact of allopurinol on contractile responses triggered by α_1-adrenergic stimulation, the CRCs of Phe (10^{-9} to 3×10^{-5} M)-induced contraction were evaluated. Relaxations to ACh are expressed as a percentage of Phe-precontracted level. Contractions to Phe are expressed as a percentage of the tone generated by KCl. Data from CRCs were plotted using the Graph Pad Software version 8.0 (San Diego, CA, USA) with sigmoid curve fitting (variable slope) performed by non-linear

regression. These curves were used to derive the values for E_{max} (the maximal relaxant response) and pEC_{50} (-log of the agonist concentration needed to produce 50% of E_{max}).

Quantitative Real-Time PCR

Total RNA from ascending aortae was extracted using Trizol© following manufacturer's recommendations (Invitrogen, USA). RNA concentration was quantified using Nanodrop (Agilent, USA). mRNA expression levels were determined by quantitative real-time PCR (qRT-PCR) using the SYBR green detection kit. mRNA levels encoding for XOR were expressed relative to GAPDH, which was used as housekeeping. qPCR reactions were performed following the protocol guidelines of the SYBR green master mix (ThermoFisher Scientific, Waltham, MA, USA). Briefly, reactions were performed in a total volume of 10 µL, including 5 µL of SYBR green PCR master mix, 2 µM of each primer, 2 µL of nuclease-free water, and 2 µL of the previously reverse-transcribed cDNA (25 ng) template on a 368-well iCycler iQ PCR plater (Bio-Rad). All reactions were carried out in duplicate for each sample. The thermocycling profile included 45 cycles consisting of denaturation at 95 ºC for 15 seconds and annealing and elongation at 60ºC for 60 seconds. Cycle threshold (Ct) values for each gene were referenced to the internal control (comparative Ct (ΔΔCt)) and converted to the linear form relative to corresponding levels in WT aortae. The primer sequences for the murine genes used in this study are shown in Table S1.

Xanthine dehydrogenase (XDH) and xanthine oxidase (XO) enzymatic activities

XO activity was determined in WT and MFS mice from liver and aorta lysates using a fluorimetry-based method (47). Part of the liver and total aorta were homogenized with 5 volumes per gram of tissue of 0.25 M sucrose, 10 mM DTT, 0.2 mM PMSF, 0.1 mM EDTA and 50 mM K-phosphate, pH 7.4. Homogenates were centrifuged for 30 min at 15,000 *g* and the supernatants were obtained for XO activity. XO activity was measured by calculating the slope of the increase in fluorescence after adding pterin (0.010 mmol/L), which measures the conversion of pterin to isoxanthopterin. XO+XDH activity was likewise determined with methylene blue (0.010 mmol/L), which replaces NAD+ as an electron acceptor. The reaction was stopped by adding allopurinol (50 µmol/L). To calibrate the fluorescence signal, the activity of a standard concentration of isoxanthopterin was measured. Values are expressed as nmol/min per g of protein. The protein concentration of homogenates was determined with the Bradford assay.

Western blotting

Total aortae from mice and dilated and non-dilated aortic zones of human patients and healthy controls were dissected and homogenized with bullet blender and beads in RIPA buffer containing 1% Triton X-100, 50 mM Tris-HCl, pH 7.5, 10 mM EGTA, 150 mM NaCl, protease inhibitors (2 mM phenylmethylsulphonyl fluoride, 10 g/L aprotinin, and 1 g/L leupeptin, 1 g/L pepstatin), and phosphatase inhibitors (2 mM Na_3VO_4 and 100 mM NaF). Samples were centrifuged at 1000 *g* for 15 min at 4 °C, the supernatants were collected, and the protein concentration was determined using the Dc protein assay kit (Bio-Rad). Proteins were denatured in 62.5 mM Tris-HCl, pH 6.8, 2%

(w/v) SDS, 10% glycerol, 140 mM mercaptoethanol, and 0.1% (w/v) bromophenol blue, heated at 100°C for 5 min, and resolved in denaturing 7% polyacrylamide gels. Proteins were transferred to nitrocellulose membranes and washed three times in Tris-buffered saline containing 0.1% Tween 20 (TBS-T). After blocking [TBS-T solution plus 5% bovine serum albumin (A9647, Sigma) and 5% skimmed milk] at room temperature for 1 h, the membranes were blotted overnight at 4°C with the following primary antibody: anti-XDX/XOR (1:500 Abcam ab109235 for human samples; 1:500 SantaCruz sc-398548 for mouse samples). After primary antibody incubation overnight, the membranes were washed with TBS-T and incubated for 1 h at room temperature with the appropriate HRP conjugated secondary antibody (1:3,000 anti-rabbit W401B antibody from Promega), and the reaction was finally visualized with the Western Blotting Luminol Reagent (Santa Cruz Biotechnology). Western blot replicates were quantified using a computer-assisted densitometric analysis (Gel-Pro Analyzer, version 4; Media Cybernetics).

Blood pressure measurements

Systolic blood pressure measurements were acquired in 9-month-old animals by the tail-cuff method and using the Niprem 645 non-invasive blood pressure system (Cibertec, Madrid, Spain). Mice were positioned on a heating pad and all measurements were carried out in the dark to minimize stress. All animals were habituated to the tail-cuff by daily training 1 week prior to the final measurements. Then, the systolic blood pressure was recorded over the course of 3 days. For quantitative analysis, the mean value of 3 measurements per day

were used for each animal. All measurements were carried out in a blinded manner with no knowledge of genotype and experimental group.

Collagen content measurements

Collagen content was evaluated with PicroSirius Red Staining method. Briefly, paraffin-embedded tissue arrays of mice aortae from different experimental sets were cut into 5 µm sections. Deparaffination was performed with xylene, and rehydration in 100% ethanol three times for 5 minutes, three times in 96% ethanol 5 min and dH_2O for 5 min. After rehydration samples were immersed in phophomolybdic acid 0,2% for 2 min and rinsed with dH_2O. Then, samples were immersed in picrosirius red (previously prepared with picric acid (Fluka 74069) and direct red 80 (Aldrich365548) for 2 h Afterwards, samples were rinsed with dH_2O for 5 min and immersed in HCl 0,01N for 2 min. To avoid background, unstaining was performed with ethanol 75º for 45 sec. Finally, slides were dehydrated with absolute ethanol for 5 min and fixated with xylene 2 times for 10 min each. Mount with DPX with coverslips. Images were captured using a Leica Leitz DMRB microscope (10x and 40x oil immersion objective) equipped with a Leica DC500 camera and analyzed with Fiji Image J Analysis software with a predesigned macro program (90).

Statistics

Data are presented either as bars showing the mean ± standard error of the mean (SEM) or boxplots, in which the error bars represent minimum and maximum values, the horizontal bars and the crosses indicate median and mean values, respectively, and the extremities of the boxes indicate interquartile

ranges. Normal distribution and equality of error variance data was respectively verified with Kolmogorov-Smirnov/Shapiro Wilk tests and Levene's test with the IBM SPSS Statistics Base 22.0 before parametric tests were used. Differences between three or four groups were evaluated using one-way or two-way ANOVA with Tukey's *post-hoc* test if data was normally distributed, and variances were equal or Kruskal-Wallis test with Dunn's *post-hoc* test was conducted if data was not normally distributed. For comparison of two groups, the unpaired t-test was utilized when the data was normally distributed, and variances were equal or the Mann-Whitney U test if data did not follow a normal distribution. A value of $P \leq 0.05$ was considered statistically significant. Data analysis was carried out using GraphPad Prism, Version 8 (GraphPad Software, La Jolla, CA).

Study approval

Human tissues were collected with the required approval from the Institutional Clinical Review Board of Spanish clinical centers, and the patients' written consent conformed to the ethical guidelines of the 1975 Declaration of Helsinki. Patients were informed about the use for research studies of their extracted aortic samples. All aortic tissues described in the manuscript are those obtained from Spanish Marfan patients and heart donors. Due to the Spanish Data Protection Act, we do not have access to their clinical history or personal data.

Animal care and colony maintenance conformed to the European Union (Directive 2010/63/EU) and Spanish guidelines (RD 53/2013) for the use of experimental animals. Ethical approval was obtained from the local animal ethics committee (CEEA protocol approval number 10340).

SUPPLEMENTAL FIGURES AND FIGURE LEGENDS

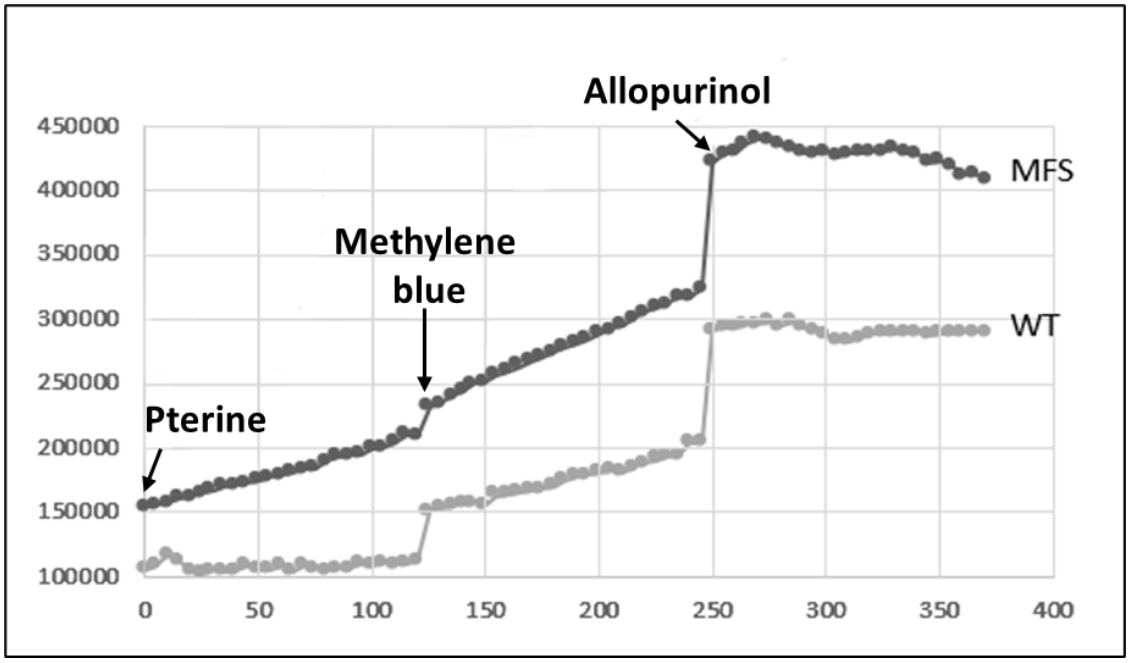

Figure S1. **Referential positive control assay for XO and XDH enzymatic activities performed in liver lysates**. WT and MFS liver lysates had pterine added as specific substrate for XO and methylene blue for total XDH (XDH +XO) activity. Allopurinol is added at the end of the assay to check its effectiveness in inhibiting total XDH activity.

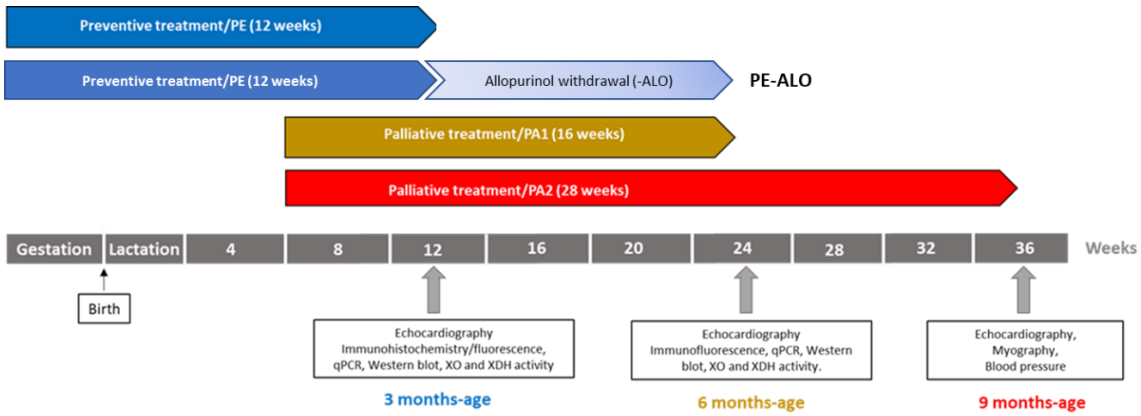

Figure S2. Representative scheme of the experimental protocols for allopurinol treatments. PE: preventive allopurinol treatment (12 weeks/3 months-age); PA: palliative allopurinol treatments PA1 and PA2. The difference between them is the duration of treatments, which for PA1 is 16 weeks (6-month-old mice) and for PA2 is 24 weeks (9-month-old mice). PE-ALO: preventive allopurinol treatment (12 weeks/3 months-age) followed by the subsequent drug withdrawal for 3 months. Endpoint at 24 weeks-age/6 months-age. Each endpoint duration protocol has a different code color, which is maintained for the figures and supplemental figures shown throughout the manuscript: blue (12 weeks/3 months-age), brown (24 weeks/6 months-age) and red (36 weeks/9 months-age).

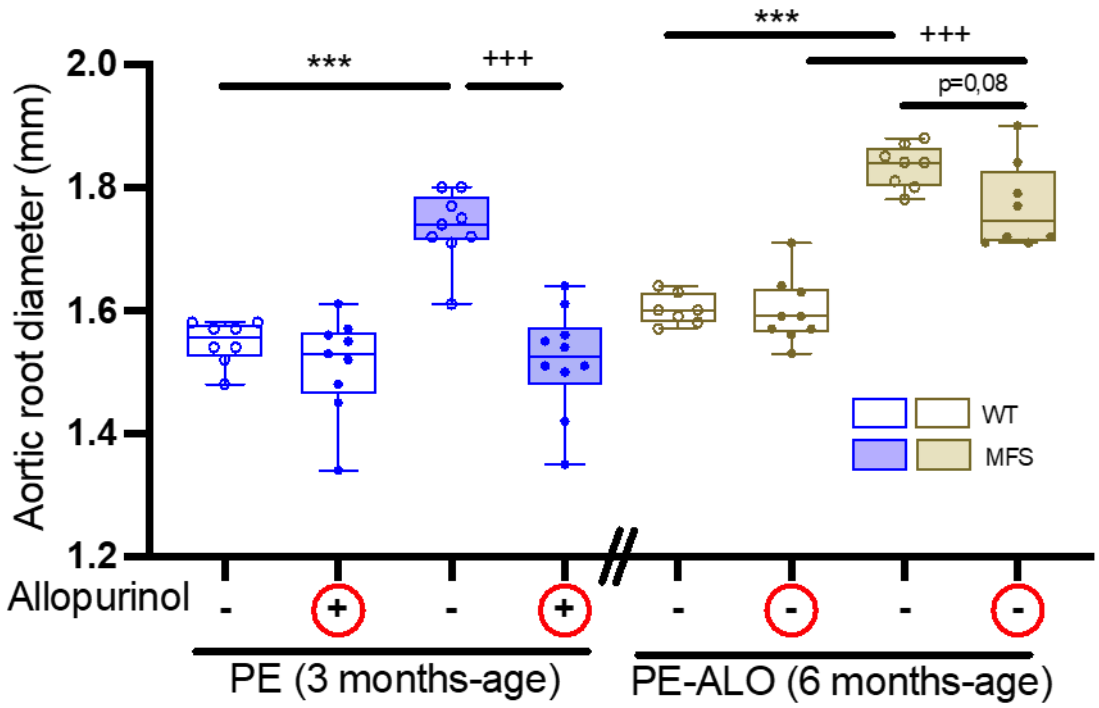

Figure S3. The aortic root dilation reappears following the withdrawal of allopurinol. WT and MFS mice were treated with allopurinol following the preventive treatment until 3 months-age (PE, 3-months-age). Thereafter, allopurinol was withdrawn from WT and MFS mice (+ inside red circles) until 6 months-age (PE-ALO) (- inside red circles). The aortic root diameter was measured by ultrasonography at 3- and 6-months-age (blue and brown boxes, respectively). N= 8-10. See also Table S4. Statistical analysis: Two-way ANOVA and Tukey post-test. ***, $^{+++}P \leq 0.001$; *effect of genotype; $^{+}$effect of treatment.

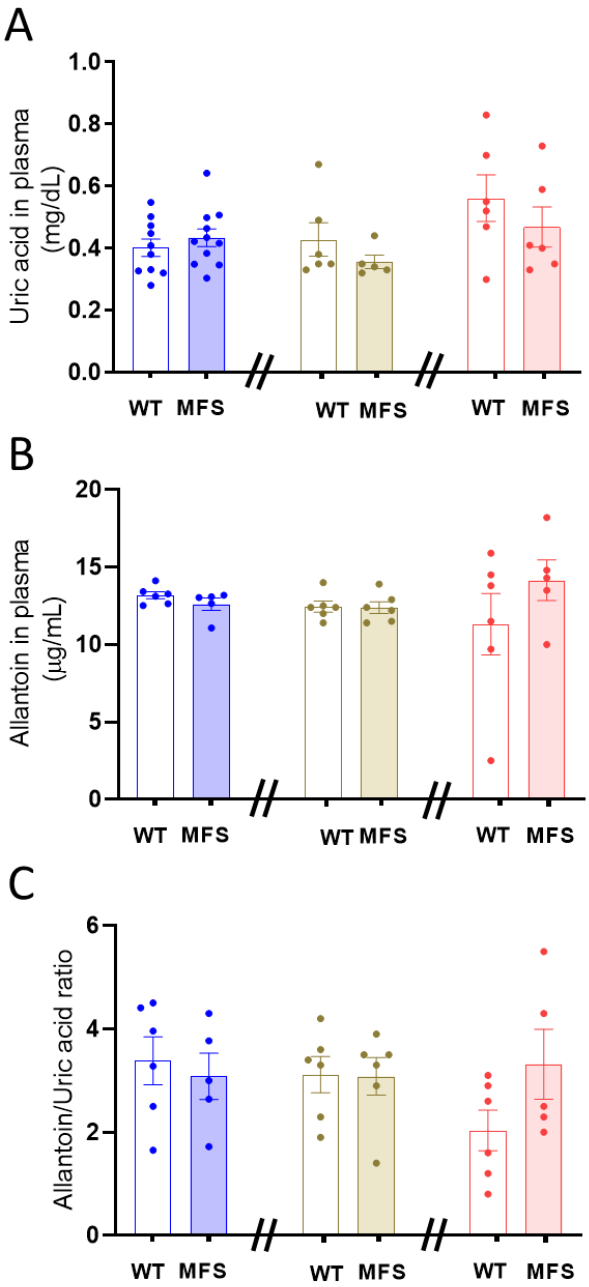

Figure S4. Uric acid and allantoin blood plasma levels are not altered in MFS mice. Blood plasma levels of uric acid (A), its catabolite allantoin (B) and their ratio (Allantoin/uric acid) (C) measured in WT and MFS mice of different ages (3-, 6-, and 9-months-old). Data as the mean ± SEM. Statistical analysis: Kruskal-Wallis with Dunn's multiple comparison test. n= 5-12.

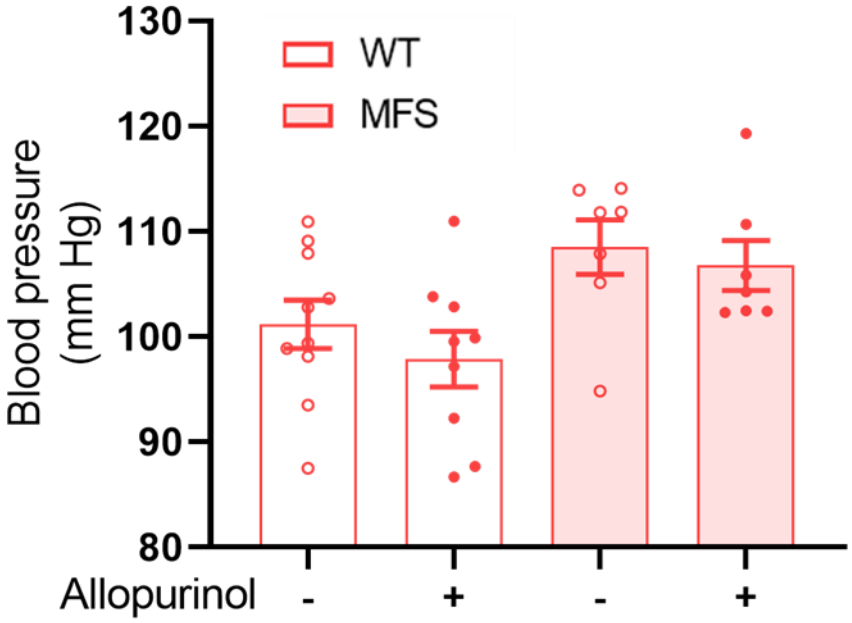

Figure S5. Allopurinol does not alter systolic blood pressure. Systolic blood pressure measurements in 9-month-old WT and MFS mice palliatively treated with allopurinol for 28 weeks (PA2) (n=6-10). Data as the mean ± SEM. Statistical analysis: Kruskal-Wallis with Dunn's multiple comparison test.

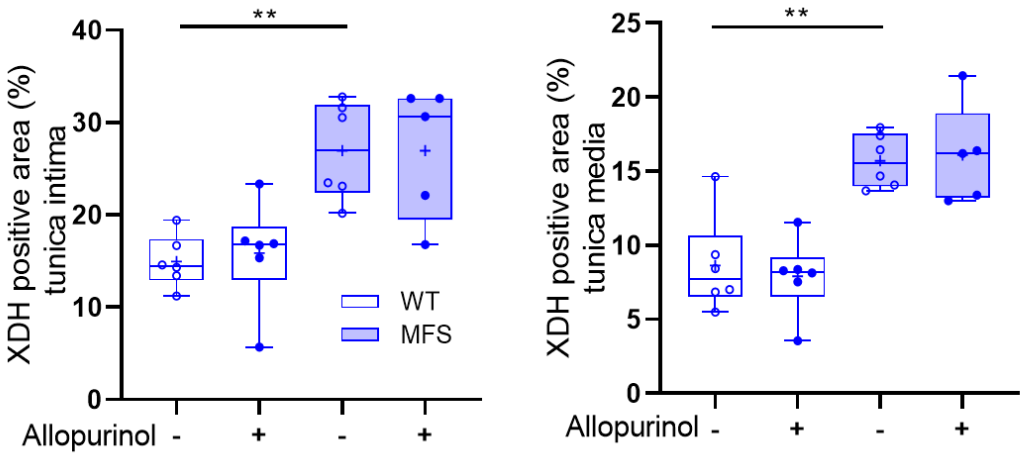

Figure S6. XDH protein levels are not affected by allopurinol treatments. Quantitative analysis of the HRP stained aortic tunicae intima and media with anti-XOR antibody of 3-month-old WT and MFS mice after preventive (PE) allopurinol treatment. Data represented as boxplots. Statistical test analyses: Two-way ANOVA and Tukey post-test. $^{**,++}P \leq 0.01$; *effect of genotype; $^{+}$effect of treatment. n=6.

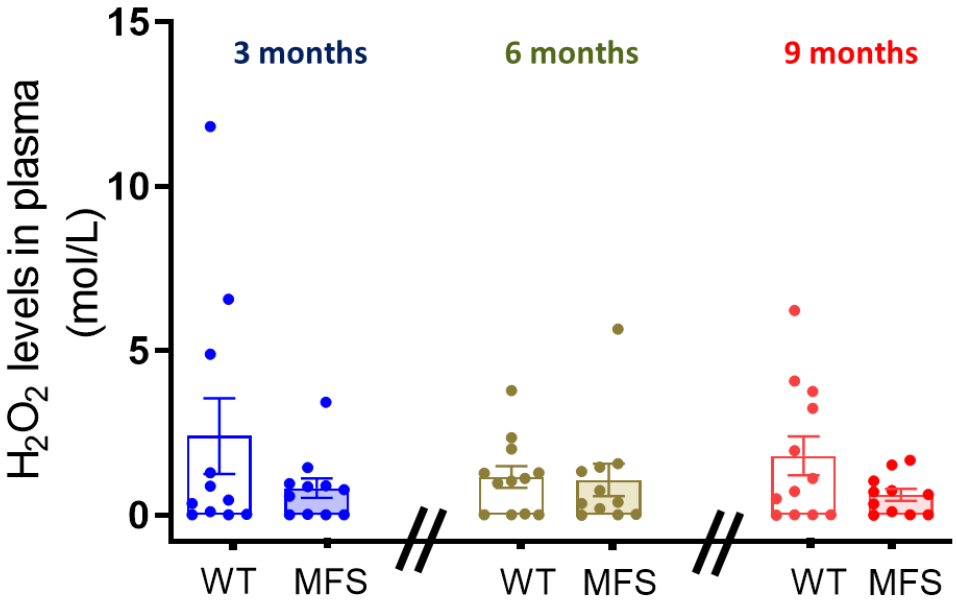

Figure S7. H_2O_2 plasma levels do not change with age in MFS mice. H_2O_2 levels in the blood plasma of WT and MFS of different ages (3-, 6-, and 9-months) (n=12-14). Data as the mean ± SEM. Statistical analysis: Kruskal-Wallis with Dunn's multiple comparison test.

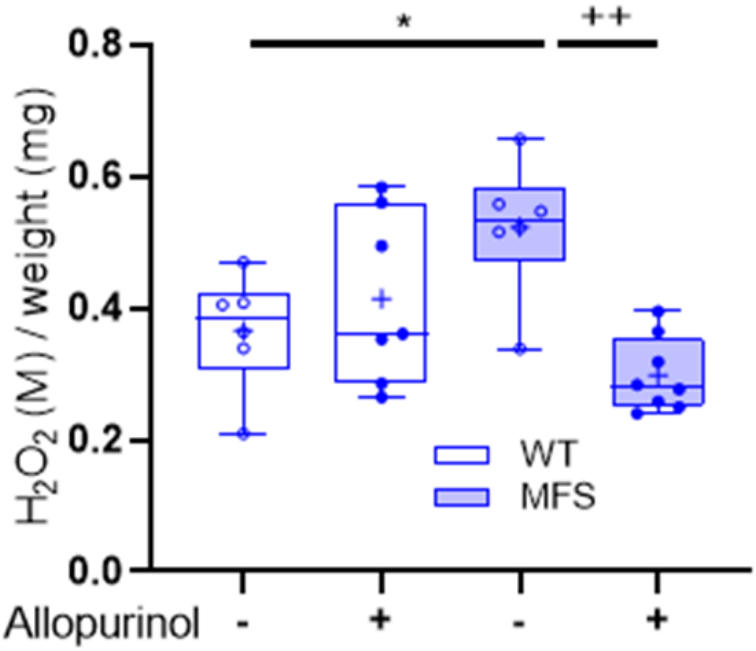

Figure S8. *In vitro* treatment of allopurinol reduces the formation of H_2O_2 in the ascending aorta of young MFS mice. Aortic rings of the part most proximal to the heart of the ascending aorta of WT and MFS mice of 3 months of age were *in vitro* treated or not with allopurinol (100 µM, final concentration) (n=6-8). Results shown here are those obtained after 2 h of allopurinol treatment. Statistical test: Kruskal-Wallis test with Dunn's multiple comparison. *$P \leq 0.05$ and $^{++}P \leq 0.01$; *effect of genotype; $^{++}$effect of treatment.

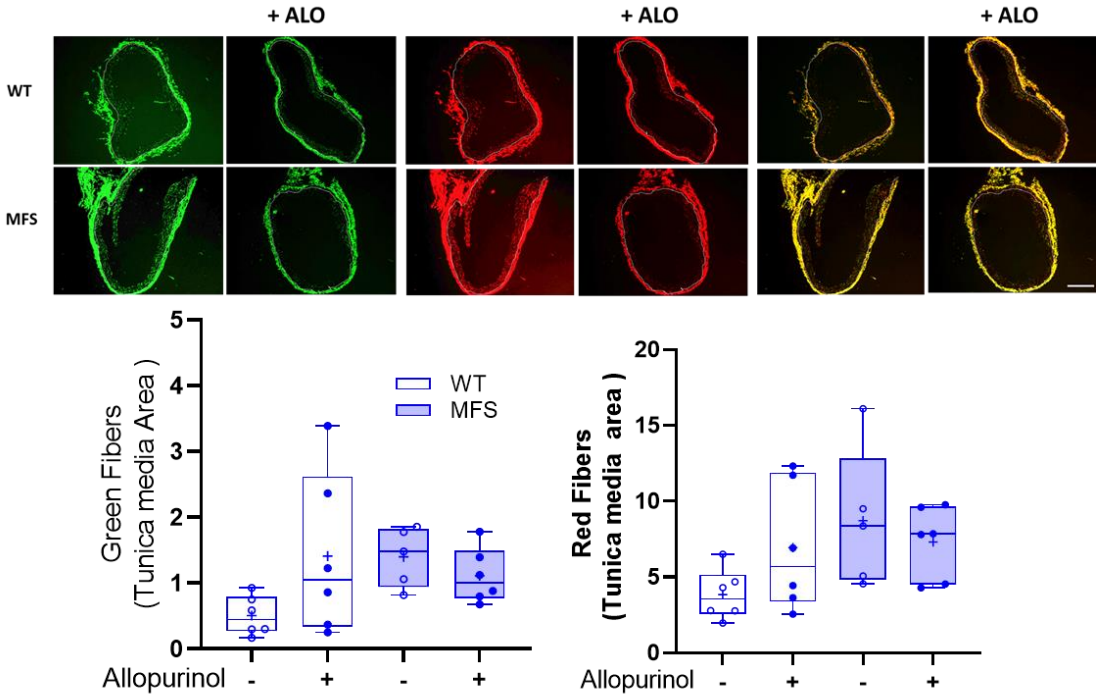

Figure S9. Preventive treatment with allopurinol does affect the collagen content and its maturation state in the media of MFS mice. Immature (green) and mature (red) collagen fibers of the tunicae media and adventitia of WT and MFS aortae stained with Picrosirius red visualized under the polarized microscope. WT and MFS mice treated or not with allopurinol in a preventive manner (PE) (n=5-6). Representative fluorescent images of the whole aorta where white dashed lines display the limit between tunicae media (inner) and adventitia (outer). The respective quantitative analysis of both types of collagen fibers is also shown. Bar, 100 µm. Data represented as boxplots. Statistical test Kruskal-Wallis and Dunn's multiple comparison tests. ***$P \leq 0.001$ and $^{+}P \leq 0.05$; *effect of genotype; $^{+}$effect of treatment.

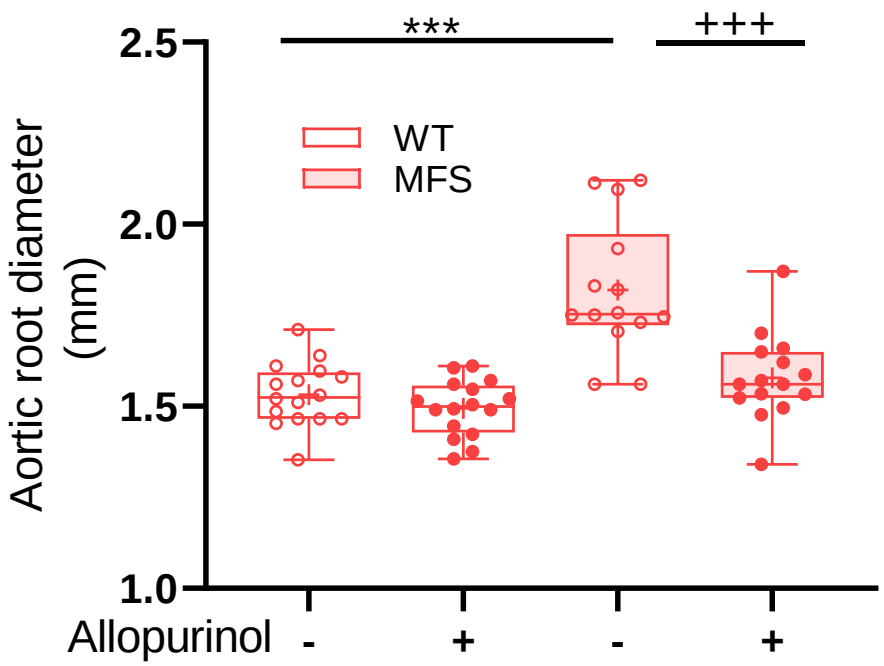

Figure S10. Aortic root diameter WT and MFS mice (9-months-old) treated or not with allopurinol for 28 weeks (PA2). Data represented as boxplots. Statistical analyses: Two-way ANOVA and Tukey post-test. ***, $^{+++}P \leq 0.001$; *effect of genotype; $^{+}$effect of treatment. n=14-16.

3. SUPPLEMENTAL TABLES

Table S1. Primers used in RT-PCR analysis in MFS mice.

Gene	Primer sequences
Xdh	Fw: 5´- GGAGATATTGGTGTCCATTGTG -3´ Rv: 5´- CCTGCTTGAAGGCTGAGAAA -3´
Gapdh	Fw: 5´- TTGATGGCAACAATCTCCAC -3´ Rv: 5´- CGTCCCGTAGACAAAATGGT-3´

Table S2. Echocardiographic values of the aortic root diameter (in mm) of WT and MFS mice subjected to palliative treatment (PA1) in the presence (+) or absence (-) of allopurinol after treatment for 16 weeks (from 8 to 24-weeks-old mice). Graphic shown in Fig. 3A. Data pooled by sex is included.

Aortic root diameter at 24-weeks-age mice (PA1)				
Allopurinol	**WT**		**MFS**	
-	**1.44±0.03**	**15**	**1.83±0.03*** **	**21**
	♂ 1.41±0.03	7	♂1.85±0.05***	11
	♀1.45±0.05	8	♀1.74±0.06***	10
+	**1.51±0.04**	**20**	**1.64±0.05^{++}**	**23**
	♂1.56±0.07	10	♂1,75±0.09	9
	♀1.45±0.03	10	♀1.57±0.04^{+}	14

Statistical analysis: Three-Way ANOVA. *effect of genotype; $^{+}$effect of treatment. ***p≤0.001; ^{++}p≤0.01; ^{+}p≤0.05. The number of animals is indicated on the right of each column. Sex: ♂ males, ♀ females. Detailed statistical analysis shown below.

Table S3. Echocardiographic values of the aortic root diameter (in mm) of WT and MFS mice subjected to preventive treatment (PE) in the presence (+) and absence (-) of allopurinol. Graphics shown in Fig. 3C.

Aortic root diameter at 12-weeks-age mice (PE)				
Allopurinol	**WT**		**MFS**	
-	1.45±0.04	11	1.71±0.04***	9
+	1.27±0.04	11	1.35±0.04^{+++}	10

Statistical analyses: Two-way ANOVA followed by Tukey post-test. *effect of genotype; $^{+}$effect of treatment. ***, $^{+++}p \leq 0.001$; $^{++}p \leq 0.01$; *$p \leq 0.05$. The number of animals is indicated on the right of each column.

Table S4. Echocardiographic values of the aortic root diameter (in mm) of WT and MFS mice subjected to preventive treatment with allopurinol (12 weeks-age/PE). Thereafter, allopurinol was withdrawn for 12 weeks and mice subjected to ultrasonography (24-weeks-age/PE-ALO). Graphics shown in Fig. S3.

	Aortic root diameter at 12 weeks-age mice (PE)				**Aortic root diameter at 24 weeks-age mice (PE-ALO)**			
Allopurinol treatment	**WT**		**MFS**		**WT**		**MFS**	
no	1.54±0.01	8	1.73±0.02***	9	1.61±0.01	7	1.84±0.01***	8
PE (12w)→PE-ALO(24w)	1.51±0.03	9	1.52±0.03^{+++}	10	1.60±0.01	9	1.77±0.02	8

Statistical analyses: Two-way ANOVA followed by Tukey post-test. *Effect of genotype; $^{+}$effect of treatment. ***,$^{+++}p \leq 0.001$. The number of animals is indicated on the right of each column.

Table S5. Echocardiographic values of the aortic root diameter (in mm) of WT and MFS mice subjected to palliative treatment (PA2) with allopurinol for 28 weeks (from 8 to 36 weeks-old mice). Data pooled for sex is also shown. Graphics shown in Fig. S10.

Aortic root diameter at 36-weeks-age mice (PA2)				
Allopurinol	**WT**		**MFS**	
-	**1.53±0.02**	**16**	**1.82±0.05*** **	**14**
	♂ 1.54±0.04	7	♂1.89±0.07***	8
	♀1.53±0.03	9	♀1.73±0.04***	6
+	**1.49±0.02**	**16**	**1.58±0.03^{+++}**	**15**
	♂1.52±0.03	7	♂1.58±0.05^{++}	8
	♀1.48±0.04	9	♀1.58±0.03^{+}	7

Statistical analysis: Three-Way ANOVA. *Effect of genotype; $^{+}$effect of treatment. ***, $^{+++}p \leq 0.001$; $^{++}p \leq 0.01$; $^{+}p \leq 0.05$. The number of animals is indicated on the right of each column. Sex: ♂ males, ♀ females.

Table S6. Potency (pEC_{50}) and maximum response (E_{max}) of the concentration–response curves (CRCs) values for ACh- and NTP-induced relaxation response (%) in the ascending aorta from WT and MFS mice (9-months-old) in the presence (+) or absence (-) of allopurinol. Graphic shown in Fig. 8D.

Ascending aorta		**WT**				**MFS**			
Allopurinol		**-**		**+**		**-**		**+**	
CRC	***E_{max} (%FE)***	88.25±2.99	6	89.70±2.52	4	82.09±4.65	6	80.06±5.45	6
ACh	***pEC_{50}***	7.52±0.10		7.69±0.08		6.85±0.13***		7.49±0.19	
CRC	***E_{max} (%FE)***	90.21±4.75	5	102.8±2.94	4	102.1±3.45	4	106.7±7.27	5
NTP	***pEC_{50}***	7.69±0.11		7.96±0.07		7.96±0.08		7.66±0.18	

*Effect of genotype; ***$p \leq 0.001$. The number of animals is indicated on the right of each column. Two-way ANOVA followed by Tukey post-test.

Table S7. KCl vascular tone was expressed as force units (mN). Potency (pEC_{50}) and maximum response (E_{max}) of the concentration-response curve (CRC) values for Phe-induced contraction response (%) in the ascending aorta of 9-month-old WT and MFS mice in the presence (+) or absence (-) of allopurinol. The number of animals is indicated on the right of each column. Graphic shown in Figs. 8B and 8E.

Ascending aorta		**WT**				**MFS**			
Allopurinol		**-**		**+**		**-**		**+**	
KCl	***E_{max} (mN)***	4.70±0.52	6	4.56±0.80	5	4.43±0.60	6	4.32±0.49	6
CRC	***E_{max} (%KCl)***	52.67±6.60	6	31.18±9.44	5	75.32±19.06	6	64.70±20.21	5
Phe	***pEC_{50}***	6.46±0.28		7.28±0.80		6.25±0.61		6.35±0.72	